Open Access

e-ISSN 2822-2938

Çukurova University Journal of Natural & Applied Sciences

CUNAS

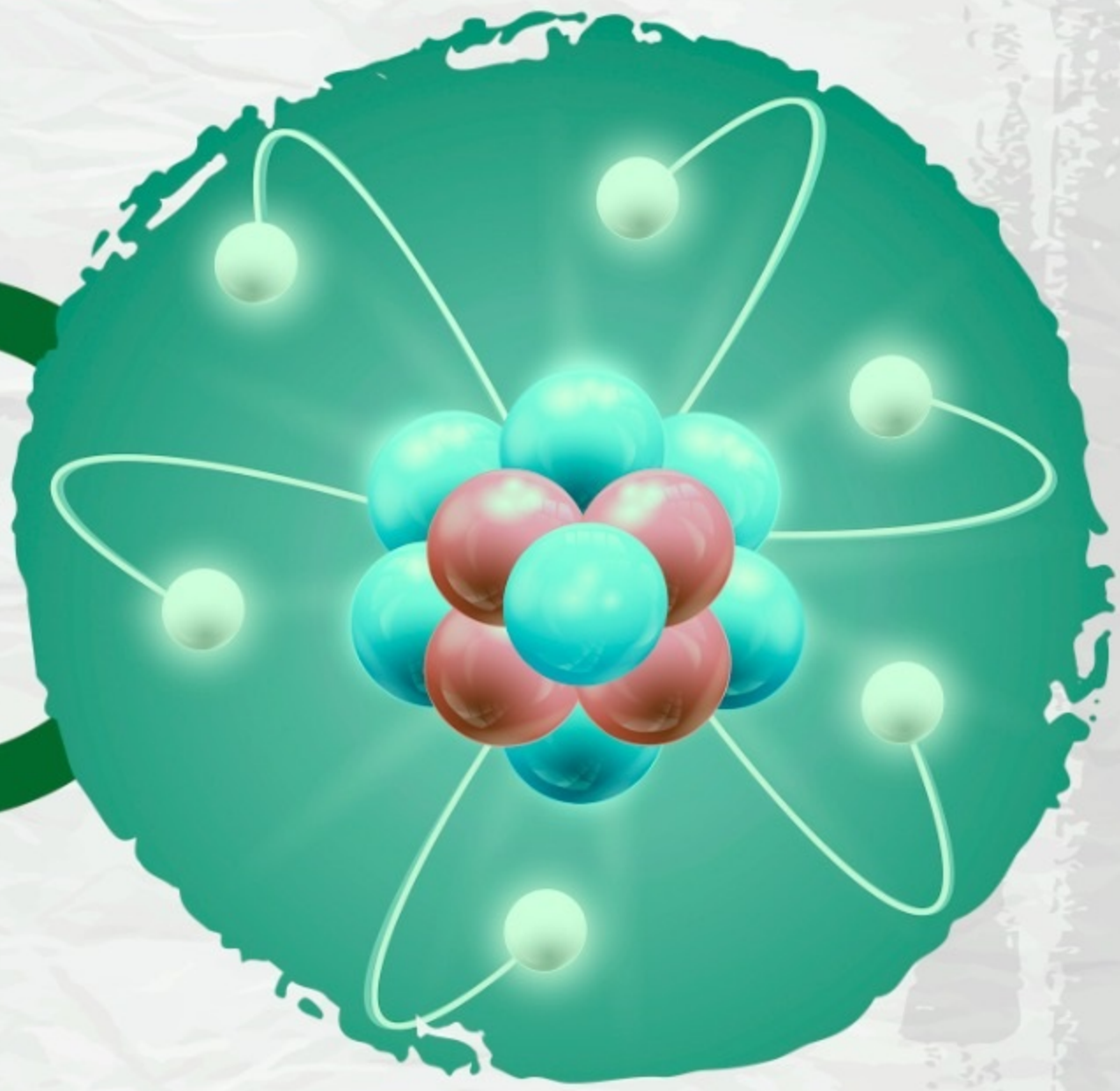

https://dergipark.org.tr/tr/pub/cunas

Sadık Dinçer
Editor-in-Chief

June 2024 - Volume 3 - Issue 1

Editorial Board

Cukurova University
Journal of
Natural & Applied Sciences

Editor in chief

Editors

Cukurova University
Journal of
Natural & Applied Sciences

Content

-Research Articles

-Review Article

Cukurova University
Journal of
Natural & Applied Sciences

Original Paper

Improving Wood Mechanical Properties Using Guinea Grass, Wood Sawdust, Crack Filler and Wood Adhesive

Dickson David OLODU[1], Andrew ERAMEH[2]

[1] Benson Idahosa University Department of Mechanical Engineering, Benin City, Edo State, Nigeria

ORCID IDs of the authors: D.D.O. 0000-0003-3383-2543; A.E. 0000-0002-6463-143X

Cite this article as: Olodu D.D., Erameh A.(2024). Improving Wood Mechanical Properties Using Guinea Grass, Wood Sawdust, Crack Filler and Wood Adhesive. Cukurova University Journal of Natural & Applied Sciences 3(1): 1-10

Abstract

Inadequate strength of plywood as a structure material have posed great challenges in its use. This research focused on the use of Guinea grass (GG), wood sawdust (SD), crack filler (CF), and wood adhesive (WA) to enhance the mechanical properties of plywood. The plywood with dimensions of 450 mm x 450 mm x 135 mm was used to produce lightweight composite slab laminates of the following dimensions: 450mm x 450mm x 145mm, 450mm x 450mm x 170mm, 450mm x 450mm x 195mm, 450mm x 450mm x 220mm, and 450mm x 450 x 245mm, respectively. To ensure tenacious bonding and lamination between the composite slab and the plywood, a wood adhesive or glue was applied evenly on the top and bottom faces of the laminates at 2.5mm thickness. Ten (10) lightweight composite slabs each were produced with mix ratios of 0.5:0.5:1.5:0.5 and 0.5:0.75:1.5:0.5 (WA: CF: SD: GG), respectively. The results obtained show that the mean compressive strength, tensile strength, density, hardness, flexural strength, and deflection of the developed laminate composite range from 74.6 N/m^2 to 76.5 N/m^2, 89.50 N/m^2 to 93.53 N/m^2, 1246.92 kg/m^3 to 1334.81 kg/m^3, 59.5 kgf to 63.5 kgf, and 7.06 N/m^2 to 7.52 N/m^2, 29.0 mm to 86.52 mm while that of plywood only ranges from 35 N/m^2 to 65 N/m^2, 45 N/m^2 to 79 N/m^2, 500 kg/m^3 to 811 kg/m^3, 32kgf to 56kgf, 2.5 N/m^2 to 6.5 N/m^2, and 20.7 mm to 45.6 mm for average compressive strength, tensile strength density, flexural strength, and deflection respectively. The results obtained show that the introduction of guinea grass, wood sawdust, crack filler, and wood adhesive improved the mechanical properties of the lightweight composite slabs developed from plywood.

Keywords: Crack Filler, Guinea Grass, Light-weight Composite Slab, Mechanical Properties, Sawdust, Wood Adhesive.

1. Introduction

In adequate investigation and production of composites made from wood as a structural material have posed great challenges in construction industries. High-performance engineered structural systems are crucial for sustainable development in the field of construction [1]. Material needed to support a weight while in use is referred to as a structural composite. Structural composites in the housing sector include load-bearing walls, roof systems, sub-flooring, staircases, framing elements, and furniture. The majority of the time, municipal or national groups' codes and specifications will outline the performance requirements for these composites [2]. The performance requirements for structural composites vary from those for the aerospace industry's high-performance materials to those for wood-based composites with lower performance demands [3]. The performance of wood-based composites differs, from expensive particle board to multi-layered plywood and laminated lumber. The low-cost adhesive used to create the structural wood-based composites meant for interior use is typically unstable to moisture. The thermosetting resin used in exterior-grade composites is more expensive than internal-grade resin but is more stable to moisture [4]. Performance can be improved in wood-based as well as agro-based composites by using chemical modification techniques to modify fiber properties such as dimensional stability, biological resistance, ultraviolet resistance, and stability to acids and bases [5]. The designed goals of fiber-reinforced composites include high strength or stiffness on a weight basis [6]. These characteristics are expressed in terms of specific strength and specific modulus parameters, which correspond to the ratios of tensile strength to specific gravity and elastic modulus to specific gravity [7].

Address for Correspondence:
Dickson David Olodu, e-mail: dolodu@biu.edu.ng

Received: May 11, 2023
Accepted: Nov 20, 2023

A slab, otherwise known as a plate, is an essential part of a structure usually found in buildings, walkways, and other civil structures. A slab that is not part of a structural frame is usually referred to as a low-sensitivity element in a structure when compared with others like beams and columns [8]. This is due to the fact that it has a larger surface area [9]. Slab as a structural element can be cast using various structural materials; some of these materials are exorbitantly priced, have a high dead weight, a high rate of yielding, have low bending strengths, degrade the environment in the course of their mining, and have other related limitations [10]. Plywood, fiber-based bamboo stick slabs, timber slabs, and composite elements such as concrete-steel reinforced slabs, steel stud-concrete decks, and particle-fibre boards are a few examples of these varied building materials [10]. The earliest type of slab was a bamboo stick slab, which was frequently employed in mud-clay homes in the 1920s and is thought to be more resistant to tensile stress than its contemporaries [11]. Physically, it has a low unit weight and high shock absorbency. The aforementioned characteristics support its application in the creation of light, self-weighted structures. In contrast to bamboo's positive attributes, it is stiff only at the nodal zone and lacks transverse strands, making it less stiff in a direction parallel to the nodes [12]. Additionally, it has a low elastic modulus [13]. Because bamboo is made up of gum, resin, and starchy materials, it needs to be properly treated with the right chemicals before being used for construction or other applications [14].

Additionally, a concrete-steel-reinforced slab is typically constructed from cement, fine aggregate (sand), coarse aggregate (often granite), steel, and water in a predetermined ratio. High compression stress resistance and resistance to microbiological and acidic assaults are two characteristics of concrete-steel-reinforced (CSR) materials. As a composite element, steel has strong tensile strength and high compression strength; therefore, being referred to as "reinforced concrete" makes it a tenacious and durable composite, cast in diverse patterns. Due to this, civil engineering projects like walkways, cover slabs, tank stands, culverts, drainage systems, bridges, and pavements have a wide range of applications [15]. Contrary to what was stated above, reinforced concrete slabs (RC) have a high dead weight, which directly raises the structure's gross weight that is transferred to the foundation and results in expensive foundation structures [16]. In a similar view, due to the rise in demand for reinforced concrete slabs, its component materials, such as granite, cement, rivers, and steel, have become highly expensive and unaffordable to average citizens [17]. Thus, the utility of industrial and agricultural waste products (such as sawdust and guinea grass) becomes valuable as they are cheap, possess a low self-weight, and pose no ecological harm [18].

This study focused on the improvement of wood mechanical properties using Guinea grass, wood sawdust, crack filler, and wood adhesive.

2. Material and Method

The materials utilized in this study are: (i) crack filler (ii) crushed guinea grass (iii) water (iv) plywood with thickness 135mm (v) wood glue.

2.1. Introduction of Materials

Crack Filler: Crack filler was purchased from the saw-mill located along airport road in Benin City, Edo State, Nigeria. The crack filler was divided into groups based on the outcomes of laboratory tests done on its physiochemical characteristics. Talc (magnesium hydroxide), kaolin, carbon, calcium carbonate, and calcium oxide (quicklime) are the chemical components of crack filler.

Plywood: The plywood was procured from a wood mill in Benin City, Edo State, Nigeria. The plywood's grade was C-grade exterior and interior veneer, and its dimensions were 450 mm x 450 mm x 135 mm (three plies, each 135 mm thick). The plywood was physically inspected to ensure there were no cracks, knots, or other defects on it. The plywood has a rough outer surface in accordance with BS EN 855-1:1994. They were sawn to 450mm by 450mm and then used to create laminated slabs with the following measurements: (a) 450mm by 450mm by 145mm; (b) 450mm by 450mm by 170mm; (c) 450mm by 450mm by 195mm; (d) 450mm by 450mm by 220mm; and (e) 450mm by 450mm by 245mm.

Wood Glue: The laminated composite slab was put together using artificial wood glue that was purchased from a wood mill in Benin City, Edo State, Nigeria. The artificial adhesive complies with ISO 656-2010 and BS 5560 [4]. The shear strength, high viscosity, high resistance to moisture, and compatibility with fillers like sawdust and powdered guinea grass were all factors in the choice of the wood glue.

Crushed Guinea Grass: The natural habitats for *Megathyrsus* maximus include open grasslands, typically in or near bushes and trees, and along riverbanks. The grass can endure both drought and wildfire. The plant exhibits significant morphological and agronomic variation, with stem lengths varying from 5 to 10 cm (2.0 to 3.9 in) and heights between 0.5 and 3.5 m (1.6 and 11.5 ft). The plant can also reproduce through apomixis, which is akin to self-cloning through seed. Panicles are open, with each plant bearing up to 9,000 seeds. This grass, when dried, possesses a light weight that can be added as a composite for structural materials.

2.2. Production Processes

Preparation and Processing of the Crushed Guinea grass: The harvested grass was washed and soaked with dilute sodium hydroxide (NaOH) of concentration 0.10 mol/dm^3 for 6 hours to ensure effective bonding between the crushed grass, sawdust, crack filler, wood glue, and plywood. The grasses were air-dried in the sun and later transferred to an oven, where they were dried at 105^{o}C. It was continuously monitored until a moisture content of about 4$\pm$0.2% was obtained [6]. The grass was crushed to granules of size 0.5 µm using a crushing machine. The crushed grass was screened to a particle size of 300 µm in diameter using a vibrating sieve machine.

Production of Plywood Laminated Composite Slab: The plywood with dimensions of 450 mm x 450 mm x 135 mm was used to produce lightweight composite slab laminates of different thicknesses (Figure 1). To ensure tenacious bonding and lamination between the composite slab and the plywood, a wood adhesive or glue was applied evenly on the top and bottom faces of the laminates at 2.5mm thickness. A total of 20 composite slabs of 10 each were produced with mix ratios of 0.5:0.5:1.5:0.5 and 0.5:0.75:1.5:0.5, respectively. The pre-mentioned water/cement ratio and blend ratio were obtained based on the high water absorption rate of the individual materials, their unit weight, their workability nature, and the need to reach the optimum strength of a light-weight composite. A manual mixing method was adopted for all slabs in order to attain good compact. The dimensions of the laminated composite slab developed were 450mm x 450mm x 145mm, 450mm x 450mm x 170mm, 450mm x 450mm x 195mm, 450mm x 450mm x 220mm, and 450mm x 450mm x 245mm, respectively (Figure 2).

Figure 1. Plywood

Figure 2. Light-weight Composite Slab

2.3. Testing Methods

Compression strength Test: The compressive strength of the lightweight composite slab was determined using a compression testing machine; a type of universal testing machine (UTM) designed specifically to assess a material's strength and deformation behavior under compressive (pressing) pressure (Figure 3). The components of this device are a load cell, a crosshead (or crossheads), compression test equipment, electronics, and a drive system. Testing software that defines machine and safety settings and stores test parameters according to testing standards like ASTM and ISO is in charge of controlling it. It is crucial to take into account both the material to be tested and the standard(s) that must be adhered to when selecting the compression test equipment. The slabs were subjected to compression test using a Magnus frame, with an attached Enerpac hydraulic pressure jack to detect its flexural strength. The compression load at yield point was recorded and was utilized to derive the flexural strength for all the slab types.

Figure 3. Digital Compression Testing Machine, Capacity: 10-300 Ton

Measurement of Density: According to ASTM D4442-92 (2003) and ASTM D2395 (2017), the density was tested. The physical characteristics of the samples were assessed on a wooden cube with the following measurements: 450 mm in length, 450 mm in thickness, and 135 mm in width. The samples were weighed to acquire the mass (m), and the sample volume at moisture content (VM) was measured using dimensional analysis. The samples were subsequently dried for 24 hours in an oven at 103 y was tested. The physical characteristics of the samples were assessed on a wooden cube with the following measurements: 450 mm in length, 450 mm in thickness, and 135 mm in width. The samples were weighed to acquire the mass (m), and the sample volume at moisture content (v) was measured using dimensional analysis. The samples were subsequently dried for 24 hours in an oven at 103 °C. They were then placed in a desiccator for about 15 minutes, or until the sample had attained a consistent oven-dry mass (m0). Using Eqn. 1, the density (ϱ) was obtained:

$$\rho = \frac{m}{v} \tag{1}$$

Tensile Test: Various samples of the lightweight laminated composite were produced at different mix ratios and were tested with strain gauge testing machines according to the requirements of the American Society for Testing and Materials (ASTM), tensile test specimens were prepared to a specified design length. ASTM E8-09 tensile standard specimens were prepared for testing. The samples prepared according to the ASTM E8M standard were carefully cleaned again from external factors such as dirt, oil and rust before the tensile test. Tensile tests were performed with a 250 kN Shimadzu universal tester at room temperature, 50±5 % humidity and 2 mm/min crosshead speed [1]. The tensile testing machine used in the experimental study is shown in Figure 5. Three individual wasted test specimens were machined from the stock having a diameter of 9 mm and a gauge length of 45 mm. The dimensions of the tensile specimens are exhibited in Figure 1. The tensile test specimens were machined to the required dimensions using the universal Lathe machine. The lightweight composite slab samples developed were evaluated for their mechanical strength (tensile strength) according to Eqn 2 [4].

$$Tensile\ Strength = \frac{\text{Maximum Load}}{\text{Original Cross-Sectional Area}} \tag{2}$$

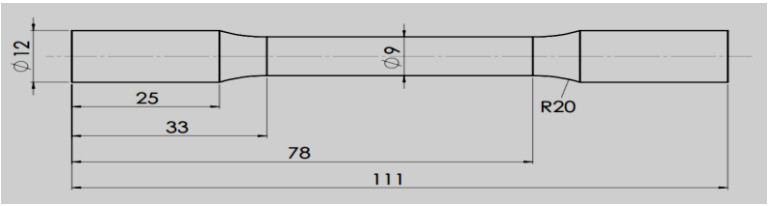

Figure 3. Dimensions of the tensile testing specimen as regard to ASTM E8-09 [1].

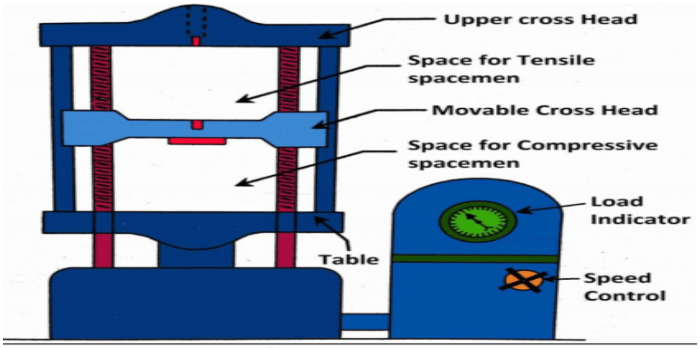

Figure 4. Universal Testing Machine

Flexural strength Test: To assess a material's ductility, bend strength, fracture strength, and resistance to fracture, bend test machines were typically universal testing devices was used. Beam specimens with the following measurements: 450 mm x 450 mm x 135 mm were made. According to IS 516-1959, two-point loading was used during testing on a 400-mm effective span. Eqn. 3 was used to compute flexural strength.

$$F = \frac{PL}{bd^2} \quad (3)$$

Where, F= Flexural strength of composite (in MPa or N/mm^2).

P= Failure load (in N).

L= Effective span of the beam (in mm).

b= Breadth of the beam (in mm).

Figure 6: Flexural Strength Testing Machine

The Brinell Hardness Test: The Brinell scale characterizes the indentation hardness of materials through the scale penetration of an indenter, loaded on a material test piece. The Brinell hardness number (HB) was then obtained using Eqn. 4 [14].

$$Brinell\ Hardness\ Number\ (BHN) - \frac{2P}{\pi D\left[D-\sqrt{D^2-d^2}\right]} \quad (4)$$

Where P is the load in kilogram, D is the steel ball diameter in millimeter, and d is the depression diameter or indentation diameter.

Figure 7. The Brinell Hardness Test Machine

3. Results and Discussion

Results for structural characteristics of composite slab made with sawdust, Crack-filler, and wood adhesive**.** The results of the structural characteristics of composite slab made with sawdust (SD), crack-filler (CF), and wood Adhesive (WA) are presented in Tables 1 to Table 4:

Table 1. Results on Compressive Strength for the Developed Light-weight Composite Slab

Mix ratio (WA:CF:SD:GG)	Sample Number	Area of Sample (mm^2)	Mass of Sample (kg)	Yield load (kN)	Compression Strength (N/mm^2)	Mean Compression strength (N/mm^2)
0.5:0.5:1.5:0.5	X1	40000	9.83	2984	74.60	
0.5:0.5:1.5:0.5	X2	40000	9.98	2980	74.50	**74.60**
0.5:0.5:1.5:0.5	X3	40000	10.13	2988	74.70	
0.5:0.75:1.5:0.5	Y1	40000	10.67	3060	76.50	
0.5:0.75 :1.5:0.5	Y2	40000	10.61	3056	76.40	**76.50**
0.5:0.75:1.5:0.5	Y3	40000	10.75	3068	76.70	

Table 2. Results on Tensile Strength for the Developed Light-weight Composite Slab

Mix Ratio (WA:CF:SD:GG)	Sample Number	Area of Sample (mm^2)	Load (kN)	Tensile Strength (N/mm^2)	Mean Tensile Strength (N/mm^2)
0.5:0.5:1.5:0.5	X1	40000	3528	88.20	
0.5:0.5:1.5:0.5	X2	40000	3580	89.50	**89.50**
0.5:0.5:1.5:0.5	X3	40000	3632	90.80	
0.5:0.75:1.5:0.5	Y1	40000	3724	93.10	
0.5:0.75:1.5:0.5	Y2	40000	3740	93.50	**93.53**
0.5:0.75:1.5:0.5	Y3	40000	3760	94.00	

Table 3. Results of Mean Density for the Developed Light-weight Composite Slab

Mix Ratio (WA:CF:SD:GG)	Sample Number	Volume of Sample (m^3)	Mass of Sample (kg)	Density (kg/m^3)	Mean Density (kg/m^3)
0.5:0.5:1.5:0.5	X1	0.008	9.83	1228.15	
0.5:0.5:1.5:0.5	X2	0.008	9.98	1245.93	**1246.92**
0.5:0.5:1.5:0.5	X3	0.008	10.13	1266.67	
0.5:0.75:1.5:0.5	Y1	0.008	10.67	1334.81	
0.5:0.75:1.5:0.5	Y2	0.008	10.61	1325.93	**1334.81**
0.5:0.75:1.5:0.5	Y3	0.008	10.75	1343.70	

Table 4. Results on Brinell Hardness for the Developed Light-weight Composite Slab

Mix Ratio (WA:CF:SD:GG)	Sample Number	Area of Sample (mm^2)	Mass of Sample (kg)	Brinell Hardness Number (N/m^2)	Mean Brinell Hardness Number (kgf)
0.5:0.5:1.5:0.5	X1	0.04	9.83	58.2	
0.5:0.5:1.5:0.5	X2	0.04	9.98	59.5	**59.5**
0.5:0.5:1.5:0.5	X3	0.04	10.13	60.8	
0.5:0.75:1.5:0.5	Y1	0.04	10.67	63.1	
0.5:0.75:1.5:0.5	Y2	0.04	10.61	63.5	**63.5**
0.5:0.75:1.5:0.5	Y3	0.04	10.75	64.0	

Table 5. Results on Flexural Strength for the Developed Light-weight Composite Slab

Slab Symbol	Mix ratio	Thickness (mm)	Yield load (kN)	Flexural strength (N/mm²)	Mean Flexural strength (N/mm²)
X1	0.5:0.5:1.5:0.5	135	225.16	7.34	**7.34**
			225.39	7.35	
X2	0.5:0.5:1.5:0.5	170	286.64	7.53	**7.52**
			285.96	7.51	
X3	0.5:0.5:1.5:0.5	195	349.44	7.43	**7.44**
			349.90	7.44	
X4	0.5:0.5:1.5:0.5	220	413.80	7.23	**7.24**
			415.00	7.25	
X5	0.5:0.5:1.5:0.5	245	484.24	7.06	**7.06**
			483.48	7.06	
Y1	0.5:0.75:1.5:0.5	135	228.44	7.48	**7.49**
			228.91	7.50	
Y2	0.5:0.75:1.5:0.5	170	286.98	7.54	**7.55**
			287.65	7.56	
Y3	0.5:0.75:1.5:0.5	195	348.52	7.41	**7.42**
			349.44	7.43	
Y4	0.5:0.75:1.5:0.5	220	415.60	7.26	**7.25**
			414.40	7.24	
Y5	0.5:0.75:1.5:0.5	245	486.52	7.09	**7.08**
			485.00	7.07	

Table 6. Results on Deflection for the Developed Light-weight Composite Slab

Slab Symbol	Mix ratio	Thickness (mm)	Yield load (kN)	Flexural Strength (N/mm²)	Deflection (mm)	Average deflection (mm)
X1	0.5:0.5:1.5:0.5	135	225.16	7.34	87.4	**86.52**
			225.39	7.35	85.9	
X2	0.5:0.5:1.5:0.5	170	286.64	7.53	74.4	**75.00**
			285.96	7.51	75.6	
X3	0.5:0.5:1.5:0.5	195	349.44	7.43	51.3	**51.00**
			349.90	7.44	50.7	
X4	0.5:0.5:1.5:0.5	220	413.80	7.23	33.4	**34.00**
			415.00	7.25	34.6	
X5	0.5:0.5:1.5:0.5	245	484.24	7.06	29.4	**29.00**
			483.48	7.06	28.6	
Y1	0.5:0.75:1.5:0.5	135	228.44	7.48	30.2	**31.00**
			228.91	7.50	31.8	
Y2	0.5:0.75:1.5:0.5	170	286.98	7.54	44.6	**44.20**
			287.65	7.56	43.8	
Y3	0.5:0.75:1.5:0.5	195	348.52	7.41	50.9	**50.70**
			349.44	7.43	50.5	
Y4	0.5:0.75:1.5:0.5	220	415.60	7.26	39.9	**40.10**
			414.40	7.24	40.3	
Y5	0.5:0.75:1.5:0.5	245	486.52	7.09	29.7	**29.90**
			485.00	7.07	30.1	

Table 7. Comparison of the Mechanical Properties of lightweight composite slab and plywood

	WOOD MATERIALS			
S/N	Mechanical Property at Mix Ratio 0.5:0.5:1.5:0.5 0.5:0.75:1.5:0.5	Produced lightweight composite slab	Plywood [1, 3, 4, 5, 8, 9, 11]	Percentage Increase in mechanical property for Produced lightweight composite slab (%)
1	Mean Compression strength (N/m²)	75.55	55	37.4
2	Average Tensile strength	91.52	70.01	24.5
3	Mean Density (kg/m³)	1290.87	770	67.6
4	Average Brinell Hardness Number (kgf)	61.50	45	36.7
5	Average Flexural strength (N/mm²)	7.34	5.87	20
6	Average deflection (mm)	47.14	40.07	15

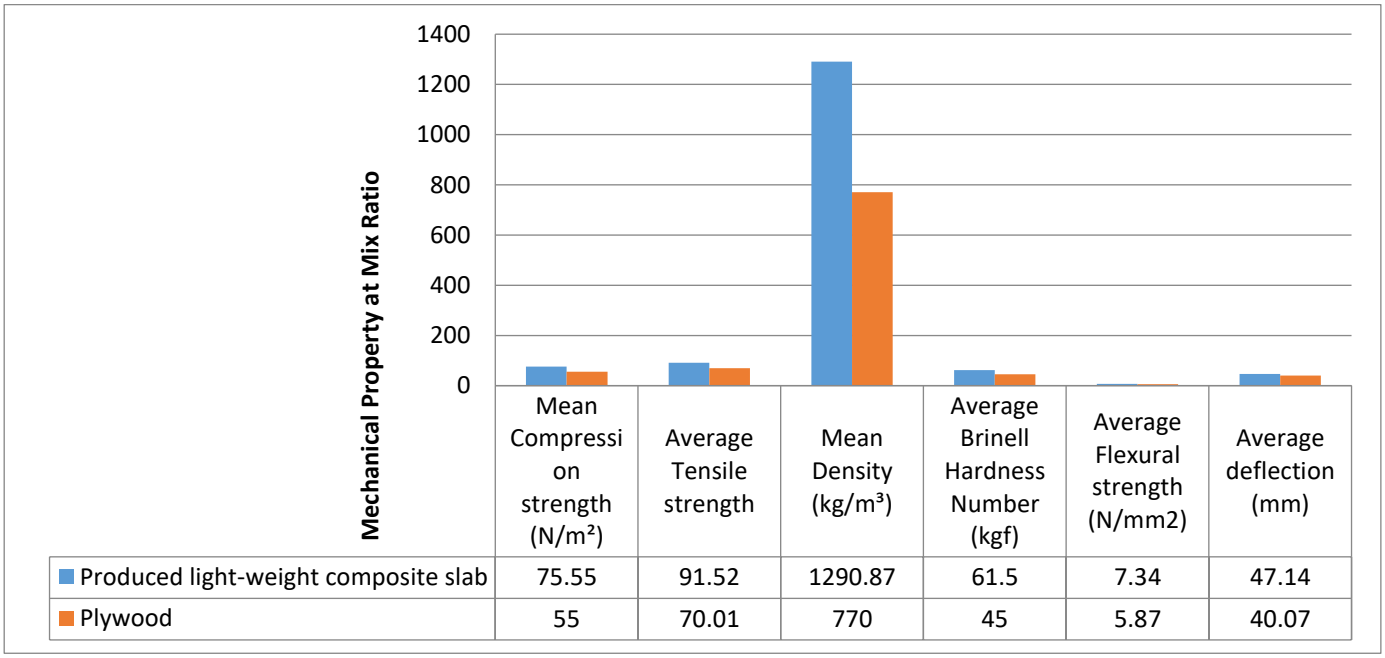

Figure 8. Mechanical Property of lightweight composite slab and plywood

3.1 Discussion of Results

The mean compressive strength of the developed lightweight slab was 74.6MPa and 76.5MPa for mix ratio 0.5:0.5:1.5:0.5 and 0.5:0.75:1.5:0.5 respectively (Table 1). The average compressive strength for both mix ratios was 75.55MPa (Table 7). The average value of the two mix ratios obtained is about 37.4% greater than the average compressive value of the timber veneer species (Mahogany, and wood specie) with about average of 55MPa for structural purposes [1, 3, 4, 5, 8, 9, 11]. The mean tensile strength of the developed lightweight slab was 89.50MPa and 93.53MPa for mix ratio 0.5:0.5:1.5:0.5 and 0.5:0.75:1.5:0.5 respectively (Table 2). The average tensile strength for both mix ratios was 91.52MPa (Table 7). The average value of the two mix ratios obtained is about 24.5% greater than the average tensile strength value of the timber veneer species (Mahogany wood specie) with about average of 70.01MPa for structural purposes [8, 9, 11]. The average density of slab density were 1246.92 Kg/m³ and 1334.81 Kg/m³ for mix ratio 0.5:0.5:1.5:0.5 and 0.5:0.75:1.5:0.5 respectively (Table 3). The average density for both mix ratios is 1290.87 kg/m³ (Table 7). The average value of the two mix ratios obtained is about 67.6% greater than the average density value of the timber veneer species (Obeche wood specie) with about average of 770kg/m³ [11]. The mean hardness of the developed light-weight slab was 59.5kgf and 63.5kgf for mix ratio 0.5:0.5:1.5:0.5 and 0.5:0.75:1.5:0.5 respectively (Table 4). The average mean hardness for both mix ratios was 61.5kgf (Table 7). The average value of the two mix ratios obtained is about 37.6% greater than the average hardness value of the timber veneer species (Iroko wood specie) with about average of 45kgf for structural purposes [8, 9, 11]. The mean flexural strength of slab for both mix ratio 0.5:0.5: 1.5:0.5 and 0.5:0.75:1.5:0.5 is in accordance with the allowable limit of the timber veneer and that of light weight element. The highest bending strength were recorded on 170mm thick slab for both mix ratios while the least bending strength were recorded on 245mm thick slab for both mix ratios. From Table 6,

the mean deflection of slab ranged from 28.9mm to 86.5mm for mix ratio 0.5: 0.5 : 1.5:0.5 and 29.85mm to 50.7mm for mix ratio 0.5: 0.75:1.5:0.5. The highest deflection were recorded on 135mm thick slab for mix ratio 0.5:0.5:1.5:0.5 and on 195mm thick slab for 0.5:0.75:1.5:0.5 while the lowest deflection were recorded on 245 mm thick slab for both blend ratios. The results obtained shows that the developed lightweight composite slab had better mechanical properties than ordinary timber veneer.

4. Conclusion

With the help of Guinea grass, wood sawdust, crack filler, and wood adhesive, the mechanical qualities of wood have been improved. The lightweight composite slabs made with mixture ratios of 0.5:0.5:1.5:0.5 and 0.5:0.75:1.5:0.5 (WA: CF: SD: GG), respectively, demonstrate how the addition of guinea grass, wood sawdust, crack filler, and wood glue enhanced the mechanical qualities of slabs made from plywood. The findings demonstrate the significance of the compressive strength, tensile strength, density, hardness, flexural strength, and average deflection of the laminate composite.

Acknowledgments

The authors acknowledged the Department of Mechanical Engineering, Faculty of Engineering, Benson Idahosa University and Igbinedion University respectively for the using some of their facilities during the fabrication process.

References

[1] Anthony, C.J. (2010). Geotechnical Mathematic Models. Masters Degree Thesis, Lousiana State university.

[2] Arbelaiz A., Fernández B., Cantero G., Llano-Ponte R., Valea A, and Mondragon I. (2005). Mechanical Properties of Flaxfibre/Polypropylene Composites. Influence of Fibre/Matrix modification and glass fibre hybridization," *Composites Part A;* 36(12):1637–1644.

[3] Azwa Z.N., Yousif B.F., Manalo A.C., and Karunasena W. (2013). A review on the degradability of polymeric composites based on natural fibres. Materials & Design; 47:424–442.

[4] Bahari, S.A., Chik, M.S., Kassim, M.A., Som Said, C.M., Misnon, M.I. and Mohamed, Z. (2012). Frictional and heat resistance characteristics of coconut husk particle filled automotive brake pad. In: American Institute of Physics Conference Series,162-168

[5] BS 4350. (1996). Wood/ Timber Glue for Structural purpose Part 1: British Standard Institute.

[6] Bulgaria Hadifa A.M., M.R. Edward M.I. (2005). Bamboo fiber filled organic composites: the influence of Filler bonding additives. Polycomposite Testing; 21:139-144

[7] Camirah, A.M., Papiro, A., Ribairo, C. (2010). Physical Properties of wood Composites; 22–24.

[8] Coutinho F.M.B., Costa T.H.S., and Carvalho D.L. (2014). Polypropylene-Wood Fiber Composites: Effect of Treatment and Mixing Conditions on Mechanical Properties. Journal of Applied Polymer Science; 65(6):1227–1235.

[9] Deepika, K., Bhaskar, R.C., Ramana, R.D. (2013). Fabrication and performance evaluation of composite material for wear resistance application. International Journal of Engineering Science and Innovative Technology; 2(6): 66-70.

[10] Espinach F.X, Julian F., Verdaguer N. (2013). Analysis of tensile and flexural modulus in Hemp Strands/Polypropylene Composites. Composites B; 47:339–343.

[11] Habiba, R., Farouk, C., and Ishleem, D.A. (2013) Properties of wood-dust Reinforced Polypropylene Composites. Journal of ModernisedScience concept and Technological Approach; 1:160-170.

[12] Jackson, J.A. (1998). mechanical Properties of Bamboo stick reinforced composite. Kluwer Academic Print.Indian standard, IS 848-2006. Wood Adhesive Standards of Plywood for concrete civil works. Specification; 2010.

[13] Liping G., Deku M.S. (1992). Production of Sawdust-Plastic Composite Using Compression Moulding" International Journal of Material Science; 2:87

[14] Nduka, N.A. (2006). Effect of Palm kernel shell as a replacement for coarse aggregate in asphaltic concrete. Journal of Engineering Practices and Technologies, 4(8):153-159.

[15] Osaremwinda J.O. and Nwachukwu J.C. (2007). Effect of particles size on some properties of Rick husk particle board'. Advanced Materials Research, Trans Tech Publication Ltd, Switzerland, pp18–19, and pp.43 – 48.

[16] Osaremwinda J.O. (2006). Effect of resin Concentration on the Properties of Groundnut Husk Particleboard", Global Journal of Mechanical Engineeing; 7(1):60-64.

[17] Pantani, R., De Santis, F., Brucato, V., Titomanlio, G. (2004). Analysis of Gate Freeze-Off Time in Injection Molding. Polymer Engineering and Science; 33(4):23-35.

[18] Parada-Soria A., Yao H.F., Alvarado-Tenorio B., Sanchez-Cadena L., and Romo-Uribe A. (2013). Recycled HDPE-Tetrapack Composites. Isothermal Crystallization, Light Scattering and Mechanical Properties. MRS Proceedings; 1485.

[19] Peterfield, B.C. (2004). Practical concrete Technology (revised edition). English University Press.

[20] Springer, Heidelberg Yahaya, A., Yakubu T., and Minasiru, T. (2009). Physical properties of sawdust from sahara region. Journal of Timber Research Vol 8(2):22-35.

[21] Yalinkilic Y., Imamura M., Tahashi H., Kalaycioglu, G., Nemli Z., Demirci and Ozdemir T. (1998). Biological, Physical and Mechanical Properties of Particleboard manufactured from waste tea leave, International Biodeterioration and Biodegradation; 41:75-84.

[22] Zaimoglu A.S., Yetimoglu T. (2012). Strength behaviour of fine grained soil reinforced with randomly distributed polypropylene fibers. Geotech Geol Eng 30(1):197–203.

[23] Zehev T. and Costas G.G. (2001). "principles of polymer processing". New York: John Wlley and sons, 2001, chapter 1 and 14.

[24] Anna, N., Siregar, I. Z., Supriyanto, Karlinasari, L., Sudrajat, D. J. (2018). Genetic variation of growth and its relationship with pilodyn penetration on the provenance-progeny trial of jabon (Neolamarkcia cadamba (Roxb) Bosser) at Parung Panjang, Bogor," J. Trop. Wood Tech. 16(2); 160-177.

[25] Anna, N., S., Karlinasari, L., Sudrajat, D.J., Siregar, I.Z. (2020). The growth, pilodyn penetration, and wood properties of 12 Neolamarckia cadamba provenances.

[26] Yongqi H., Vincent J.L., Gan, H.C. (2020). Behavior of a Two-Way Lightweight Steel–Concrete Composite Slab Voided with Thin-Walled Core Boxes towards Sustainable Construction. Materials; 13(18):4129; https://doi.org/10.3390/ma13184129

Cukurova University
Journal of
Natural & Applied Sciences

Original Paper

In vitro Cytogenotoxic Effects of a Coumarin-Selenophene Hybrid Compound

Hasan Basri ILA[1]

[1] Department of Biology, Faculty of Science and Letters, Çukurova University, Adana, Turkey

ORCID IDs of the authors: H.B.I. 0000-0002-3221-8587.

Cite this article as: Ila H.B. (2024). In vitro Cytogenotoxic Effects of a Coumarin-Selenophene Hybrid Compound. Cukurova University Journal of Natural & Applied Sciences 3(1): 11-18

Abstract

This study was carried out to reveal the in vitro cytogenotoxic effect of 2-amino-5-(6-bromo-2-oxo-2H-chromen-3-yl) selenophene-3-carbonitrile (6-BrCoumSel or CoumSel), a newly synthesized coumarin-selenophene hybrid compound. Coumarin (2H-chromen-2-one), one of the main components of the test substance hybrid molecule (CoumSel), is an aromatic organic chemical compound with the formula $C_9H_6O_2$. Pharmacologically, coumarin belongs to the flavonoid group of chemicals. The other component, selenophene, has the formula C_4H_4Se and is an unsaturated organic compound containing a five-membered ring containing selenium in its structure. It is a colorless liquid and is one of the most common selenium heterocycles. It was found that in human lymphocytes cultured *in vitro*, the hybrid CoumSel compound increased the frequency of chromosome abnormalities (CA) and micronuclei (MN), especially at high concentrations, compared to the untreated group (0 µg/ml). However, the increase in MN in the 200 µg/ml 48-hour treatment was statistically significant. The notable cytotoxic effects were detected at high concentrations. The potential of CoumSel as an antiproliferative drug with its current properties should not be ignored.

Keywords: Coumarin-selenophene hybrid compound, in vitro human lymphocyte, chromosome aberration, micronucleus, cytotoxicity.

1. Introduction

Found in many plants, including some edible plants, coumarin is a pleasant-smelling natural flavoring substance. It has extensive use in the pharmaceutical and cosmetics industry but is partially toxic to the liver and kidneys. LD_{50} rat: 293 mg/kg (Figure 1) [1].

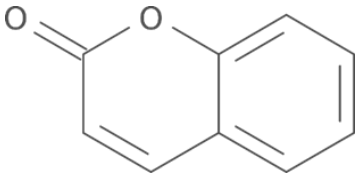

Figure 1. Coumarin (benzo-α-pyrone)

Although slightly dangerous to humans, coumarin is hepatotoxic in rats, but this toxicity has been reported to be less in mice. Metabolism in rodents converts coumarin into a more dangerous and unstable byproduct, causing liver cancer in rats and lung tumors in mice [2,3]. Although coumarin is a negative mutagen in in vivo studies, it has been demonstrated that it has both promutagenic properties and can increase the effects of some promutagens by increasing micronucleus stimulation in *in vitro* cells stimulated with S9 [4,5]. While some coumarin derivatives showed significant cytotoxic effects due to apoptosis in cancer cell lines like MCF-7, HeLa, etc., they did not show cytotoxic effects in the healthy cell line (HEK-293). It has been stated that these

Address for Correspondence:
Hasan Basri Ila, e-mail: hasanbasriila@gmail.com

Received: Feb 14, 2024
Accepted: Mar 8, 2024

compounds are promising antimicrobial agents against pathogenic strains of Pseudomonas aeruginosa and Candida albicans, which were examined to evaluate their antimicrobial effects [6–8]. Coumarin and its derivatives are an anticoagulant drug prescribed to reduce the risk of blood clotting, venous thrombosis, and pulmonary embolism by inhibiting vitamin K synthesis [9]. Vitamin K is an activator of coagulation factors II, VII, IX, and X, so as the amount of vitamin K decreases, the synthesis of these factors also decreases. Coumarin is an oral anticoagulant that inhibits Vitamin K epoxide reductase, an enzyme that recycles oxidized vitamin K [10]. Coumarin and its derivatives are preferred in the pharmaceutical industry because they show antioxidant, antitumor, and anti-inflammatory activity. Some coumarin derivatives constitute the active ingredient of insecticides. Cause of its pleasant smell is also used in foodstuffs, soaps, perfumes, and other cleaning products. Moreover, coumarin is utilized as an optical brightening in the structure of laser and fluorescence dyes [11].

The other component of the test substance (CoumSel) is selenophene, which has the formula C4H4Se. Selenophene is an unsaturated organic compound containing a five-membered ring carrying selenium. The selenophene molecule is straight and aromatic and is subject to electrophilic substitution reactions at the -2 or -2.5 positions. This structure may have brought some properties to selenophene. These reactions are slower than furan but faster than thiophene. The first confirmed production of selenophene was achieved by Mazza and Solazzo in 1927 by heating acetylene and selenium together at approximately 300°C [12,13].

Selenophene is a biologically active compound with hepatoprotective, antinociceptive (pain relieving), anticonvulsant [14], antihypertensive [15], and antitumoral [16] properties. Compounds containing selenophene are extremely useful synthetic intermediates (Figure 2). They can serve as suitable building blocks to synthesize other biologically active compounds.

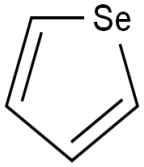

Figure 2. Selenophene [17]

Some of the selenophene-derived compounds showed anticancer [18,19], antiradical/antioxidant [20–22], and antiestrogenic activity [23,24]. Some selenophene-derived compounds exhibit potent cytotoxic/apoptotic properties with broad-spectrum antitumor activity [25–28]. An enhanced activity of the selenophene analog molecule against DNA gyrase has been documented [29]. Again, tert-butyl benzo[b]tellurophen-2-ylmethylcarbamate, a selenophene derivative, caused inhibition of histone H3 lysine 9 demethylase (KDM4) in HeLa cells but did not show such an effect in healthy cells [30].

The selenium contained in the selenophene compound participates in the structure of different compounds in soil, plants, and water. It is vital for organisms. It is a structural element of many enzymes, notably glutathione peroxidase, which protects cell membranes from oxidative damage. The chemical form of selenium, the selenium level of the organism, and the number of elements that interfere with selenium metabolism or increase the requirement in the diet, such as sulfur, vitamin E, lipids, amino acids, proteins, cadmium, mercury, copper and arsenic, determine the need for selenium. Selenium deficiency can cause different abnormalities in humans. However, excessive selenium intake can also cause poisoning [31].

This study was conducted to reveal the genotoxic and cytotoxic label of the newly synthesized coumarin-selenophene derivative molecule (CoumSel), which has the potential to be used for different purposes in many industrial fields and whose biological effect potential has not yet been adequately evaluated. The studies were conducted with peripheral blood cultures obtained from healthy volunteers under *in vitro* conditions. The genotoxicity and cytotoxicity findings detected provided significant results regarding this chemical. Considering the potential of the existing chemical to be used in many industrial areas, the results of the scientific study will provide an analytic perspective for the future projection of CoumSel.

2. Material and Method

2.1. Test Substance (6-Br- CoumSel or CoumSel)

The test substance in the study, the coumarin-selenophene hybrid compound, 6-bromo salicylaldehyde (6-Br-CoumSel) molecule, was synthesized in the organic chemistry laboratory of Cukurova University Arts and Science Faculty Department of Chemistry

as follows: Initially, coumarin compounds were synthesized by Pechmann and Knoevenagel methods. Then, the 2-amino selenophene-3-carbonitrile molecule was synthesized by the Gewald method, and coumarin-selenophene hybrid derivatives were prepared [11].

The test concentrations were determined by conducting preliminary experiments under in vitro conditions with this newly synthesized derivative chemical. In the study, we tried to reveal an insight related to the genotoxic potential of the test chemical by investigating in vitro chromosome aberration (CA) and micronucleus (MN) induction in peripheral lymphocytes. The cytotoxic effect of the test substance by mitotic index (MI) and nuclear division index (NDI) data were analyzed.

Chemical name: 2-amino-5-(6-bromo-2-oxo-2H-chromen-3-yl) selenophene-3-carbonitrile

Chemical formula: C14H7BrN2O2Se

Nickname: CoumSel (Figure 3)

Molecular weight: 394.08 g/mol

Solubility: Dimethyl sulfoxide (DMSO)

Physical appearance: Solid, brown

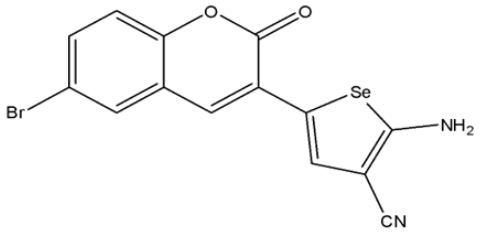

2-amino-5-(6-bromo-2-oxo-2*H*-chromen-3-yl)selenophene-3-carbonitrile

Figure 3. Coumsel

2.2. Chemicals

Colchicine (CAS No: 64–86–8), cytochalasin B (CAS 14930–96–2), Mitomycin C (MMC) (CAS 50–07–7), and DMSO (CAS 67-68-5) were purchased from Sigma-Aldrich Company (Steinheim, Germany).

2.3. Experimental design and statistical analysis

To perform this work, the permits were obtained from the Cukurova University Ethics Committee (06 March 2020/97, Decision No: 16). Human peripheral blood was taken from nonsmokers four healthy volunteers (two males and two females [ages: 21 and 24]) with an intravenous needle. Human blood culture was treated with CoumSel at 0, 50, 100, or 200 μg/mL concentrations for one or two cell cycle periods (24 h or 48 h). The highest concentration was determined with OECD TG 473 and TG 489 protocols. According to this protocol, the recommended highest concentration should show 55 ± 5% cytotoxicity. Dimethyl sulfoxide (DMSO) as the solvent control and mitomycin C (MMC) as well as the positive control were used in the experiments. All values were reported as means ± standard error (SE); we analyzed the data using the One-Way Analysis of Variance (ANOVA) LSD post hoc test and SPSS software (IBM SPSS Statistics 25). The concentration-response effects we determined using the Pearson correlation. In group comparisons, the standard level of significance is $P \leq 0.05$.

2.4. Chromosome Abnormality (CA) Test

To examine the cytogenetic effects of 6-bromo-CoumSel, used as the test substance, we applied four different concentrations (0, 50, 100, and 200 μg/mL) to the healthy peripheral blood culture for 24 or 48 hours. Since the test substance did not dissolve homogeneously in distilled water, we dissolved it in DMSO, an organic solvent. To block mitosis in the metaphase stage, 0.06 µg/mL of the colchicine solution was added to each tube at the 70th hour of the culture period, and the tubes were mixed by gently shaking. We pretreated cells with colchicine for 2 hours at 37°C. At the end of the 72nd hour, we harvested and stained the cells from culture tubes, as stated by Arslan et al. [32].

The 100 well-distributed c-metaphases in homogeneously stained preparations were examined to detect chromosomal abnormalities (CA) in each variant. To determine the mitotic index (MI), we calculated the percentage of dividing cells at 3000 cells.

$$MI(\%) = \frac{number\ of\ cells\ in\ mitosis}{total\ number\ of\ cells} x100 \quad (1)$$

2.5. Micronucleus (MN) Test

The cultured human peripheral lymphocytes were treated with four concentrations of the chemical 6-bromo-CoumSel for 24 or 48 hours. At the end of the culture period, we prepared micronucleus slides for each variant according to the method of Arslan et al. [32].

To detect micronucleated cells in prepared preparations, we examined 1000 binucleated cells. To calculate the nucleus division index (NDI), we determined the cells with 1, 2, 3, and 4 nuclei among 1000 cells and applied the following formula.

$$NDI = \frac{[(1\ x\ M1) + (2\ x\ M2) + (3\ x\ M3) + (4\ x\ m4)]}{N\ (total\ number\ of\ cells)} \quad (2)$$

3. Results

3.1. Chromosome abnormality (CA) findings

It was found that the CA values caused by the test substance (CoumSel) were at the level of the DMSO and 0 µg/ml groups. Slight rises in CA findings related to enhanced CoumSel concentration were not meaningful and were within confidence limits. Moreover, we could not observe a safe number of metaphases in the 48-hour treatment of the highest concentration (200 µg/mL) due to the possible toxic effect on the culture, so we did not include it in the statistical analysis. Abnormality levels per cell (CA/cell) showed similarities to CA% values (Table 1). As with CA%, there were no notable differences in CA/cell ($P>0.05$). On the other hand, we confirmed the cytotoxic effect potential of the test substance. In particular, the increase in CoumSel concentration caused significant cytotoxic effects at both treatment periods (24 and 48 hours). The highest concentration of CoumSel (200 µg/ml) showed a cytotoxic effect compared to the negative (0 µg/mL) control in the 24-hour application ($P<0.001$). It was statistically confirmed that this cytotoxic effect occurs at the MMC level. Again, 100 µg/mL CoumSel exhibited significant cytotoxic potential compared to both the DMSO control and 0 µg/ml groups in the 48-hour treatment ($P<0.001$) (Table 1).

Table 1. Chromosome aberrations percentage (CA%), CA/cell ratio, and mitotic index (MI) in human-cultured lymphocytes treated with CoumSel.

Test Substance	Treatment		*CA%±SE	CA/cell ±SE	**MI±SE
	Time (hour)	Cons. (µg/mL)			
MMC	24	0.25 µL/mL	35.25 ± 1.25	0.525 ± 0.018	2.57 ± 0.26 a3
DMSO	24	10 µL	1.00 ± 0.00	0.010 ± 0.000	6.22 ± 0.23 a3
CoumSel	24	0	1.25 ± 0.25 a3	0.012 ± 0.002 a3	7.39 ± 0.47 a3 b2
CoumSel	24	50	1.50 ± 0.28 a3	0.015 ± 0.003 a3	6.69 ± 0.13 a3
CoumSel	24	100	1.50 ± 0.28 a3	0.015 ± 0.003 a3	7.00 ± 0.11 a3
CoumSel	24	200	1.75 ± 0.25 a3	0.017 ± 0.002 a3	3.28 ± 0.12 c3
MMC	48	0.25 µL/mL	62.00 ± 2.19	2.250 ± 0.237	1.15 ± 0.16
DMSO	48	10 µL	0.50 ± 0.28	0.005 ± 0.003	7.24 ± 0.29
CoumSel	48	0	1.25 ± 0.25 a3	0.012 ± 0.002 a3	7.39 ± 0.47 a3
CoumSel	48	50	1.75 ± 0.47 a3	0.017 ± 0.005 a3	7.60 ± 0.11 a3
CoumSel	48	100	2.00 ± 0.40 a3	0.020 ± 0.004 a3	5.00 ± 0.3 a3b3c3
CoumSel	48	†200	-	-	-

3.1. Micronucleus (MN) findings

In the study, 200 µg/mL, 48-hour CoumSel application significantly increased the MN‰ rate compared to the negative control (0 µg/mL) group ($P<0.001$). The MN per binuclear cell (MN/binuclear cell) ratio caused by the test substance shows a similar trend to the MN‰ ratio. Nuclear division indices (NDI) are negatively related to the test substance concentration, but the dose-effect correlation is not statistically significant. The highest cytotoxic effects occurred at 100 µg/mL and 200 µg/mL. CoumSel in

these concentrations significantly reduced the NDI value in both treatment periods (24 or 48 hours) compared to both the solvent (DMSO) control and the negative control group (P<0.001) (Table 2)

Table 2. Effect of CoumSel on the ratios of micronucleus (MN), MN/binuclear cell, and nuclear division index (NDI) in human-cultured lymphocytes

Test Substance	Treatment		*MN‰±SE	MN/Binuclear cell ±SE	NDI±SE
	Time (hour)	Cons. (µg/ml)			
MMC	24	0.25 µL/mL	23.50 ± 1.041	0.228 ± 0.014	1.245 ± 0.051
DMSO	24	10 µL	6.00 ± 0.408	0.006 ± 0.000	1.483 ± 0.029
CoumSel	24	0	3.25 ± 0.479 a3	0.003 ± 0.000 a3	1.367 ± 0.030 a2b2
CoumSel	24	50	4.00 ± 0.408 a3	0.004 ± 0.000 a3	1.433 ± 0.009 a3
CoumSel	24	100	3.50 ± 0.289 a3	0.004 ± 0.000 a3	1.309 ± 0.016 b3
CoumSel	24	200	5.75 ± 1.031 a3	0.006 ± 0.001 a3	1.185 ± 0.023 b3c3
MMC	48	0.25 µL/mL	130.75 ± 4.990	0.109 ± 0.000	1.095 ± 0.015
DMSO	48	10 µL	2.75 ± 0.250	0.003 ± 0.000	1.338 ± 0.052
CoumSel	48	0	3.25 ± 0.479 a3	0.003 ± 0.000 a3	1.367 ± 0.030 a3
CoumSel	48	50	3.50 ± 0.289 a3	0.004 ± 0.000 a3	1.309 ± 0.016 a3
CoumSel	48	100	2.50 ± 0.289 a3	0.003 ± 0.000 a3	1.196 ± 0.014 a1b3c3
CoumSel	48	†200	13.00 ± 0.577 a3b3c3	0.013 ± 0.014 a3	1.126 ± 0.004 b3c3

*: Examined 1000 cells in each donor, 4000 cells in total. †: Calculated from a total of 3000 cells. a: The difference is significant compared to the positive (MMC) control. b: The difference is significant compared to the solvent (DMSO) control. c: The difference is significant compared to the untreated (0 µg/ml) control. a1b1c1≤ 0.05, a2b2c2≤ 0.01, a3b3c3≤ 0.001.

4. Discussion and Conclusion

The in vitro cytogenotoxic effect hypothesis of the coumarin-selenophene hybrid compound (CoumSel) was tested with in vitro human peripheral lymphocytes. Experiments revealed that chromosome aberration (CA) and micronucleus (MN) frequencies increased, especially in cells where high concentrations were applied, but only the MN increase at 200 µg/mL concentration was significant. There are many effects underlying the emergence of this result. These may be oxidative activity on DNA or microtubule (mitotic spindle) structure, covalent binding affinity to the DNA backbone, or topoisomerase enzyme inhibition effect. In addition, the various agents on enzymes or auxiliary factors involved in DNA replication or repair or nucleotide monomers may cause genotoxicity. According to the results of an old study confirming this idea, monofunctional and bifunctional pyrroles increased sister chromatid exchange (SCE), which is an indicator of genotoxicity in human lymphocytes, and especially bifunctional pyrroles were more effective in increasing SCE [33]. A different study reported similar results. According to the results of this study, two of the three commercially available partially photo-treated pyrrole-derived intermediates (1H-pyrrole-2-carboxaldehyde and 6-chloro-2-pyridinecarboxylic acid) are genotoxic even at low concentrations, while 2-pyridinecarbonitrile is only cytotoxic [34].

The tautomeric conformation of any biomolecule is determined by the combination and distribution of electrical charges of the atoms that make up that molecule. Any proton or electron shifts in the molecule may unpredictably affect its standard stability, causing it to transform into a different conformational form. This situation can directly or indirectly affect the molecule and prevent its optimized function. Unstable oxygen species (ROS), described as reactive in aerobic respiring cells, attack all biomolecules, including nucleic acids, and can disrupt their characteristic electrical dynamics. This phenomenon, called oxidative stress, can result in the molecule's unique function being restricted or completely blocked. It has long been known that the primary origin of oxidizing products is electron leaks in the mitochondrial respiratory chain (ETS). Many studies investigating the effects of oxidative interactions on genome stability released significant outputs. These findings include genomic instability of the cell and activation or inactivation of various biochemical mechanisms. DNA lesions or molecular dysfunctions resulting from reactive attack may cause cell cycle arrest and apoptotic cell death. Briefly, it is undeniable that the multicomponent mitotic machinery that ensures cell division is de facto affected by oxidative stress [35–42]. Test substance CoumSel may have had cytotoxic effects through different mechanisms. Erşatır et al. stated that Coumsel, a coumarin and 2-aminoselenophene-3-carbonitrile derivative, showed significant cytotoxic and antiproliferative effects on the MCF-7 cell line. The same researchers found that contrary to

popular belief, these coumarin derivatives have a radical scavenging (antioxidative) effect, not an oxidative one [43]. It could not find any reliable study on the direct oxidative effect of coumarin selenophene derivative compounds.

According to the mitotic index (MI) and nuclear division index (NDI) data I determined in my study, CoumSel showed cytotoxic effects, especially at high concentrations. This observed effect may be due to genotoxicity because they share a similar underlying pattern. However, there are also minor variational differences in our findings. Although no definite clastogenic effect is observed, the increase in MN frequency highlights the aneugenic effect of the test substance. I suggest oxidative or nonoxidative impacts on the cell division apparatus (mitotic spindle, centromere, etc.) as the reason for this. The cytotoxicity in our study may have arisen from confusion in the spindle apparatus. It is known that tubulin-binding molecules interfere with the dynamic balance of microtubules, destroying microtubule reorganization in the M phase and forming abnormal spindles. This causes cell cycle arrest, leading to apoptotic cell death [44].

In summary, the genotoxic and cytotoxic effects of CoumSel at high concentrations are remarkable. With this anti-mitotic feature, it may provide new insight into the solution to the problem of uncontrolled cell proliferation. Additionally, focusing on different experiments that will reveal the metabolic action of the test chemical will expand the scientific perspective.

Acknowledgment

I thank CUBAP for this support. Moreover, I especially thank Büşra Boz for evaluating the experimental data and the other researchers who contributed to our project (Dr. Giray and Dr. Erşatır).

References

[1] Merck Coumarin., n.d. Coumarin msds. Coumarin MSDS - 822316 - Merck. https://www.merckmillipore.com/TR/tr/product/msds/MDA_CHEM-822316. [accessed November 28, 2023].

[2] Born, S.L., Api, A.M., Ford, R.A., Lefever, F.R., Hawkins, D.R., (2003). Comparative metabolism and kinetics of coumarin in mice and rats. Food and Chemical Toxicology. 41(2): 247–58. doi: 10.1016/S0278-6915(02)00227-2.

[3 Vassallo, J.D., Hicks, S.M., Daston, G.P., Lehman-McKeeman, L.D., (2004). Metabolic Detoxification Determines Species Differences in Coumarin-Induced Hepatotoxicity. Toxicological Sciences. 80(2): 249–57. doi: 10.1093/TOXSCI/KFH162.

[4] Kishino, Y., Hasegawa, T., Arakawa, S., Shibaya, Y., Yamoto, T., Mori, K., (2019). Effect of the metabolic capacity in rat liver S9 on the positive results of in vitro micronucleus tests. The Journal of Toxicological Sciences. 44(3): 145–53. doi: 10.2131/JTS.44.145.

[5] Kanode, R., Chandra, S., Sharma, S., (2017). Application of bacterial reverse mutation assay for detection of non-genotoxic carcinogens. Toxicology Mechanisms and Methods. 27(5): 376–81. doi: 10.1080/15376516.2017.1300616.

[6] Dhawan, S., Awolade, P., Kisten, P., Cele, N., Pillay, A.S., Saha, S.T., et al., (2020). Synthesis, Cytotoxicity and Antimicrobial Evaluation of New Coumarin-Tagged β-Lactam Triazole Hybrid. Chemistry & Biodiversity. 17(1). doi: 10.1002/CBDV.201900462.

[7] Maleki, E.H., Bahrami, A.R., Sadeghian, H., Matin, M.M., (2020). Discovering the structure–activity relationships of different O-prenylated coumarin derivatives as effective anticancer agents in human cervical cancer cells. Toxicology in Vitro. 63: 104745. doi: 10.1016/J.TIV.2019.104745.

[8] Ahmed, E.Y., Abdel Latif, N.A., El-Mansy, M.F., Elserwy, W.S., Abdelhafez, O.M., (2020). VEGFR-2 inhibiting effect and molecular modeling of newly synthesized coumarin derivatives as anti-breast cancer agents. Bioorganic & Medicinal Chemistry. 28(5). doi: 10.1016/J.BMC.2020.115328.

[9] Verhoef, T.I., Redekop, W.K., Daly, A.K., Van Schie, R.M.F., De Boer, A., Maitland-Van Der Zee, A.H., (2014). Pharmacogenetic-guided dosing of coumarin anticoagulants: algorithms for warfarin, acenocoumarol and phenprocoumon. British Journal of Clinical Pharmacology. 77(4): 626. doi: 10.1111/BCP.12220.

[10] www.drugs.com (What are Coumarins)., n.d. List of Coumarins and indandiones - Drugs.com. https://www.drugs.com/drug-class/coumarins-and-indandiones.html. [accessed January 22, 2024].

[11] Erşatır, M., Giray, E.S., (2018). Fen ve Mühendislik Bilimleri Dergisi Yıl: 35–41.

[12] Hartough, H.D. (Howard D., Hochgesang, F.P. (Frank P.)., Blicke, F.F. (Frederick F., (1952). Thiophene and its derivatives: 533.

[13] Eicher, T., Hauptmann, S., Speicher, A., (2003). The Chemistry of Heterocycles. The Chemistry of Heterocycles. doi: 10.1002/352760183X.

[14] Wilhelm, E.A., Jesse, C.R., Bortolatto, C.F., Nogueira, C.W., Savegnago, L., (2009). Anticonvulsant and antioxidant effects of 3-alkynyl selenophene in 21-day-old rats on pilocarpine model of seizures. Brain Research Bulletin. 79(5): 281–7. doi: 10.1016/J.BRAINRESBULL.2009.03.006.

[15] Grange, R.L., Ziogas, J., North, A.J., Angus, J.A., Schiesser, C.H., (2008). Selenosartans: novel selenophene analogues of milfasartan and eprosartan. Bioorganic & Medicinal Chemistry Letters. 18(3): 1241–4. doi: 10.1016/J.BMCL.2007.11.136.

[16] Juang, S.H., Lung, C.C., Hsu, P.C., Hsu, K.S., Li, Y.C., Hong, P.C., et al., (2007). D-501036, a novel selenophene-based triheterocycle derivative, exhibits potent in vitro and in vivo antitumoral activity which involves DNA damage and ataxia telangiectasia-mutated nuclear protein kinase activation. Molecular Cancer Therapeutics. 6(1): 193–202. doi: 10.1158/1535-7163.MCT-06-0482.

[17] Merck-Selenophene., n.d. Selenophene 97 288-05-1. https://www.sigmaaldrich.com/TR/en/product/aldrich/367141. [accessed January 22, 2024].

[18] Mhetre, A.B., Lee, H., Yang, H., Lee, K., Nam, D.H., Lim, D., (2017). Synthesis and anticancer activity of benzoselenophene and heteroaromatic derivatives of 1,2,9,9a-tetrahydrocyclopropa[c]benzo[e]indol-4-one (CBI). Organic & Biomolecular Chemistry. 15(5): 1198–208. doi: 10.1039/C6OB02729F.

[19] Adly, M.E., Gedawy, E.M., El-Malah, A.A., El-Telbany, F.A., (2019). Synthesis and Anticancer Activity of Certain Selenophene Derivatives. Russian Journal of Organic Chemistry. 55(8): 1189–96. doi: 10.1134/S1070428019080189/METRICS.

[20] Schumacher, R.F., Rosário, A.R., Souza, A.C.G., Acker, C.I., Nogueira, C.W., Zeni, G., (2011). The potential antioxidant activity of 2,3-dihydroselenophene, a prototype drug of 4-aryl-2,3-dihydroselenophenes. Bioorganic & Medicinal Chemistry. 19(4): 1418–25. doi: 10.1016/J.BMC.2011.01.005.

[21] Singh, V.P., Yan, J., Poon, J.F., Gates, P.J., Butcher, R.J., Engman, L., (2017). Chain-Breaking Phenolic 2,3-Dihydrobenzo[b]selenophene Antioxidants: Proximity Effects and Regeneration Studies. Chemistry – A European Journal. 23(60): 15080–8. doi: 10.1002/CHEM.201702350.

[22] Tavadyan, L.A., Manukyan, Z.H., Harutyunyan, L.H., Musayelyan, M. V., Sahakyan, A.D., Tonikyan, H.G., (2017). Antioxidant Properties of Selenophene, Thiophene and Their Aminocarbonitrile Derivatives. Antioxidants. 6(2). doi: 10.3390/ANTIOX6020022.

[23] Luo, J., Hu, Z., Xiao, Y., Yang, T., Dong, C., Huang, J., et al., (2017). Rational design and optimization of selenophenes with basic side chains as novel potent selective estrogen receptor modulators (SERMs) for breast cancer therapy. MedChemComm. 8(7): 1485–97. doi: 10.1039/C7MD00163K.

[24] Zhang, S., Wang, Z., Hu, Z., Li, C., Tang, C., Carlson, K.E., et al., (2017). Selenophenes: Introducing a New Element into the Core of Non-Steroidal Estrogen Receptor Ligands. ChemMedChem. 12(3): 235. doi: 10.1002/CMDC.201600593.

[25] Juang, S.H., Lung, C.C., Hsu, P.C., Hsu, K.S., Li, Y.C., Hong, P.C., et al., (2007). D-501036, a novel selenophene-based triheterocycle derivative, exhibits potent in vitro and in vivo antitumoral activity which involves DNA damage and ataxia telangiectasia-mutated nuclear protein kinase activation. Molecular Cancer Therapeutics. 6(1): 193–202. doi: 10.1158/1535-7163.MCT-06-0482.

[26] Shiah, H.S., Lee, W.S., Juang, S.H., Hong, P.C., Lung, C.C., Chang, C.J., et al., (2007). Mitochondria-mediated and p53-associated apoptosis induced in human cancer cells by a novel selenophene derivative, D-501036. Biochemical Pharmacology. 73(5): 610–9. doi: 10.1016/J.BCP.2006.10.019.

[27] Yang, Y.N., Chou, K. ming., Pan, W.Y., Chen, Y. wen., Tsou, T.C., Yeh, S.C., et al., (2011). Enhancement of non-homologous end joining DNA repair capacity confers cancer cells resistance to the novel selenophene compound, D-501036. Cancer Letters. 309(1): 110–8. doi: 10.1016/J.CANLET.2011.05.023.

[28] Csuk, R., Siewert, B., Wiemann, J., (2013). A bioassay-driven discovery of an unexpected selenophene and its cytotoxicity. Bioorganic & Medicinal Chemistry Letters. 23(12): 3542–6. doi: 10.1016/J.BMCL.2013.04.036.

[29] Wiles, J.A., Phadke, A.S., Bradbury, B.J., Pucci, M.J., Thanassi, J.A., Deshpande, M., (2011). Selenophene-containing inhibitors of type IIA bacterial topoisomerases. Journal of Medicinal Chemistry. 54(9): 3418–25. doi: 10.1021/JM2002124/SUPPL_FILE/JM2002124_SI_001.PDF.

[30] Kim, Y.J., Lee, D.H., Choi, Y.S., Jeong, J.H., Kwon, S.H., (2019). Benzo[b]tellurophenes as a Potential Histone H3 Lysine 9 Demethylase (KDM4) Inhibitor. International Journal of Molecular Sciences. 20(23). doi: 10.3390/IJMS20235908.

[31] Çetïn, M., Denïz, G., Polat, Ü., Yalçin, A., (2002). Broylerlerde inorganik ve organik selenyum ilavesinin biyokimyasal kan parametreleri üzerine etkisi. Vet. Med. 21: 59–63.

[32] Arslan, M., Timocin, T., Ila, H.B., (2017). In vitro potential cytogenetic and oxidative stress effects of roxithromycin. Drug and Chemical Toxicology. 40(4): 463–9. doi: 10.1080/01480545.2016.1264410.

[33] Ord, M.J., Herbert, A., Mattocks, A.R., (1985). The ability of bifunctional and monofunctional pyrrole compounds to induce sister-chromatid exchange (SCE) in human lymphocytes and mutations in Salmonella typhimurium. Mutation Research. 149(3): 485–93. doi: 10.1016/0027-5107(85)90167-8.

[34] Skoutelis, C., Antonopoulou, M., Konstantinou, I., Vlastos, D., Papadaki, M., (2017). Photodegradation of 2-chloropyridine in aqueous solution: Reaction pathways and genotoxicity of intermediate products. Journal of Hazardous Materials. 321: 753–63. doi: 10.1016/J.JHAZMAT.2016.09.058.

[35] Limoli, C.L., Giedzinski, E., (2003). Induction of chromosomal instability by chronic oxidative stress. Neoplasia (New York, N.Y.). 5(4): 339–46. doi: 10.1016/S1476-5586(03)80027-1.

[36] Cooke, M.S., Evans, M.D., Dizdaroglu, M., Lunec, J., (2003). Oxidative DNA damage: mechanisms, mutation, and disease. FASEB Journal : Official Publication of the Federation of American Societies for Experimental Biology. 17(10): 1195–214. doi: 10.1096/FJ.02-0752REV.

[37] Barzilai, A., Yamamoto, K.I., (2004). DNA damage responses to oxidative stress. DNA Repair. 3(8–9): 1109–15. doi: 10.1016/j.dnarep.2004.03.002.

[38] Salmon, T.B., Evert, B.A., Song, B., Doetsch, P.W., (2004). Biological consequences of oxidative stress-induced DNA damage in Saccharomyces cerevisiae. Nucleic Acids Research. 32(12): 3712–23. doi: 10.1093/NAR/GKH696.

[39] Gonzalez-Hunt, C.P., Wadhwa, M., Sanders, L.H., (2018). DNA damage by oxidative stress: Measurement strategies for two genomes. Current Opinion in Toxicology. 7. doi: 10.1016/j.cotox.2017.11.001.

[40] Walczak, C.E., Heald, R., (2008). Mechanisms of mitotic spindle assembly and function. International Review of Cytology. 265: 111–58. doi: 10.1016/S0074-7696(07)65003-7.

[41] Przewloka, M.R., Glover, D.M., (2009). The kinetochore and the centromere: a working long distance relationship. Annual Review of Genetics. 43: 439–65. doi: 10.1146/ANNUREV-GENET-102108-134310.

[42] Gabel, C.A., Li, Z., DeMarco, A.G., Zhang, Z., Yang, J., Hall, M.C., et al., (2022). Molecular architecture of the augmin complex. Nature Communications 2022 13:1. 13(1): 1–13. doi: 10.1038/s41467-022-33227-7.

[43] Erşatır, M., Yıldırım, M., Giray, E.S., Yalın, S., (2020). Synthesis and antiproliferative evaluation of novel biheterocycles based on coumarin and 2-aminoselenophene-3-carbonitrile unit. Monatshefte Fur Chemie. 151(4): 625–36. doi: 10.1007/S00706-020-02573-X/TABLES/7.

[44] Budhiraja, A., Kadian, K., Kaur, M., Aggarwal, V., Garg, A., Sapra, S., et al., (2012). Synthesis and biological evaluation of naphthalene, furan and pyrrole based chalcones as cytotoxic and antimicrobial agents. Medicinal Chemistry Research. 21: 2133–40. doi: 10.1007/s00044-011-9733-y.

Cukurova University
Journal of
Natural & Applied Sciences

Original Paper

Oxidative stress status of freshwater fish (*Oreochromis niloticus*) exposed to cadmium in differing calcium levels

Mustafa Canli[1]

[1]Çukurova University, Faculty of Sciences and Arts, Department of Biology, Adana, Turkey

ORCID IDs of the authors: M.C. 0000-0002-7038-6186.

Cite this article as: Canli M. (2024). Oxidative stress status of freshwater fish (Oreochromis niloticus) exposed to cadmium in differing calcium levels. Cukurova University Journal of Natural & Applied Sciences 3(1): 19-24

Abstract

Xenobiotic exposures cause an alteration in oxidative stress in fish and metals are one of the most toxic xenobiotics present in the environment. Thus, freshwater fish (*Oreochromis niloticus*) were exposed to Cd in different calcium levels (30, 60 and 120 mg/L), resembling the waters with different hardness. Experiments were conducted in 2 different durations, denoted acute (25 μM Cd, 3 days) and chronic (5 μM Cd, 30 days) and the serum of fish was used to measure the oxidative status. For this aim, total oxidant status (TOS) and total antioxidant status (TAS) were measured in the serum and associated oxidative stress indicator values (OSI) were calculated. Data showed that Cd exposures, at all calcium levels, did not cause any fish mortality or changes in feeding behaviour. Likewise, the oxidative stress parameters did not change significantly ($p>0.05$) among controls. However, the mean TOS values between controls and Cd-exposed fish differed significantly ($p<0.05$), as there were increases in TOS values in fish. Similarly, the mean TAS values between controls and Cd-exposed fish also differed significantly ($p<0.05$), as there were decreases in TAS values. OSI values significantly increased in Cd-exposed fish, suggesting oxidative stress. Data showed that significant alterations in the measured parameters were seen more at the lower calcium levels, emphasizing the protective roles of calcium ions against the toxic effects of Cd. This study demonstrated the effective and fast determinations of metal toxicity in fish regarding oxidative stress status and suggested that be used in environmental monitoring.

Keywords: Metal, Cadmium, Calcium, Fish, Oxidative, Antioxidant.

1. Introduction

The aquatic environments are contaminated by different xenobiotics worldwide, causing serious environmental problems. Therefore, these systems must be controlled using different methods, including the biological responses of aquatic animals. In particular, rivers and lakes seem to be more affected by industrial or domestic effluents, as they have small volumes and are located in human settlement areas [1,2]. Metals or metal-containing products are a group of xenobiotics which threaten the aquatic biota, causing serious problems [3-5].

Several biomarker molecules belonging to different metabolic systems are used to detect the stress that fish face after metal exposures, naming them as "early warning systems" before hazardous effects occur [6,7,8,9]. There is a natural balance between free radicals and antioxidant defence systems in aerobic organisms. If this balance shifts towards free radicals, oxidative stress occurs. There are very important enzymes or non-enzymatic substances synthesized in cells to eliminate oxidant substances either taken from outside (e.g. heavy metals and pesticides) or produced by the organism itself (reactive oxygen derivatives, etc.). One of the important antioxidant enzymes such as superoxide dismutase, catalase, glutathione peroxidase and glutathione S-transferase. On the other hand, substances such as alpha-tocopherol (vitamin E), ascorbic acid (vitamin C), beta-carotene, flavonoid, coenzyme Q and lycopene have non-enzymatic antioxidant properties. In addition to measuring many enzymatic and non-enzymatic parameters one by one, scientists may achieve quick and easy methods to determine oxidative stress by measuring TOS and TAS together with OSI values [10,11].

Thus, the present study was undertaken to investigate the effects of cadmium on the oxidative stress status of freshwater fish (*O. niloticus*). Experiments were carried out in acute (3 days 25 μM Cd) and chronic (30 days, 5 μM Cd) durations at different calcium levels (30, 60 and 120 mg Ca/L). Then, the TOS and TAS values in the serum were measured and associated OSI values (arbitrary unit) were calculated to determine the oxidative stress status of fish.

Address for Correspondence:
Mustafa Canli, e-mail: mcanli@cu.edu.tr

Received: Feb 14, 2024
Accepted: Apr 2, 2024

2. Material and Method

2.1. Experimental Protocol

Freshwater fish (*O. niloticus*) are continuously cultured in the pools of the Fisheries and Aquatic Sciences Faculty at Cukurova University (Adana, Turkiye). Fish were transferred from the pools to the ecotoxicology laboratory situated in the Biology Department and placed in glass aquariums (40x40x100 cm) to let them accustomed to the new conditions for one month. The physical and chemical conditions in the laboratory are presented in Table 1. The experimental room was air-conditioned (21±1.0 °C) and enlightened with fluorescent lamps (daylight 65/80 W) for 12 hours. The tab water used for the experiment had a pH value of 8.0±0.3 and a total hardness of 231±2.2 $CaCO_3$, oxygen levels of 5.7±0.87 mg O_2/L. Fish were fed once a day with fish food supplied from Pinar Yem (Izmir, Turkiye). The mean length (15.4±1.33cm) of fish used in the experiments did not differ significantly (P>0.05) among controls and exposure groups. The chemicals used in the present study were supplied from Merk Company (Germany).

Table 1. Data (mean±sd) show the physical and chemical conditions of 3 control waters depending on their calcium levels (Ca_{30}, Ca_{60} and Ca_{120}) during the experiments

Parameters	Ca_{30}	Ca_{60}	Ca_{120}
Calcium (mg Ca/L)	28.3±0.56	58.3±0.86	115.8±1.52
Tot. hardness (mg $CaCO_3$/L)	98.6±6.76	192±7.54	355±16.5
Alkalinity (mg $CaCO_3$/L)	99.0±2.34	98.9±4.23	103±5.22
Conductivity (µS/cm)	170±5.55	303±4.34	610±9.97
Oxygen (mg/L)	5.90±0.28	6.02±0.26	6.21±0.28
Temperature (°C)	20.5±0.33	21.0±0.55	19.9±0.25
pH	7.08±0.07	7.10±0.06	6.99±0.04

Experiments were carried out using spring waters supplied by Nestle company (Nestle Pure Life), as they had very low Ca levels (30 mg/L). This water was used as background calcium levels and then, calcium levels of the water were increased to 60 and 120 mg Ca/L by adding $CaCl_2$ appropriately, to obtain soft, mild and hard water. Thus, there were 3 controls with different calcium levels (Ca_{30}, Ca_{60} Ca_{120}). Finally, fish were exposed to Cd (as CdCl) for 3 days (25 µM Cd) for acute experiments and 30 days (5 µM Cd) for chronic experiments. For each exposure concentration and control, 6 fish (a total of 60 fish) were used and the media were changed every 3rd day to supply clean water and re-load Cd and calcium. After acute and chronic durations, fish were removed from the aquariums and killed by the transaction of the spinal cord (permission of the Ethic Committee of Cukurova University). Blood samples were immediately taken by puncture of the caudal vessel and centrifuged at 3000 × g (Hettich Universal 30 RF, Germany) for 5 min (4 °C) to obtain the serum. Then, the serum samples were frozen at -85 °C (Esco UUS-480A) for later measurements of TAS and TOS values. Total oxidant and total antioxidant levels in serum were measured by spectrophotometer (Shimadzu UV-1800) using Rel Assay Diagnostic kits. The oxidative effects of cadmium and/or calcium were determined by the method of Erel [12,13].

Statistical Analyses

A statistical package program (SPSS 20) was performed to analyze the data. Acute and chronic exposures were handled separately and results were accepted if $p<0.05$. First, data were checked for their normality. Considering the results of this test, One-way ANOVA test or Kruskal-Wallis One-Way ANOVA test was applied to the data to estimate differences among control and cadmium exposure groups. Data showing significant differences were re-tested by Tukey or Mann-Whitney U test to determine group differed from the individual control group. Mean values and associated standard errors were shown in figures (Figures 1-3), indicating the results of statistical tests.

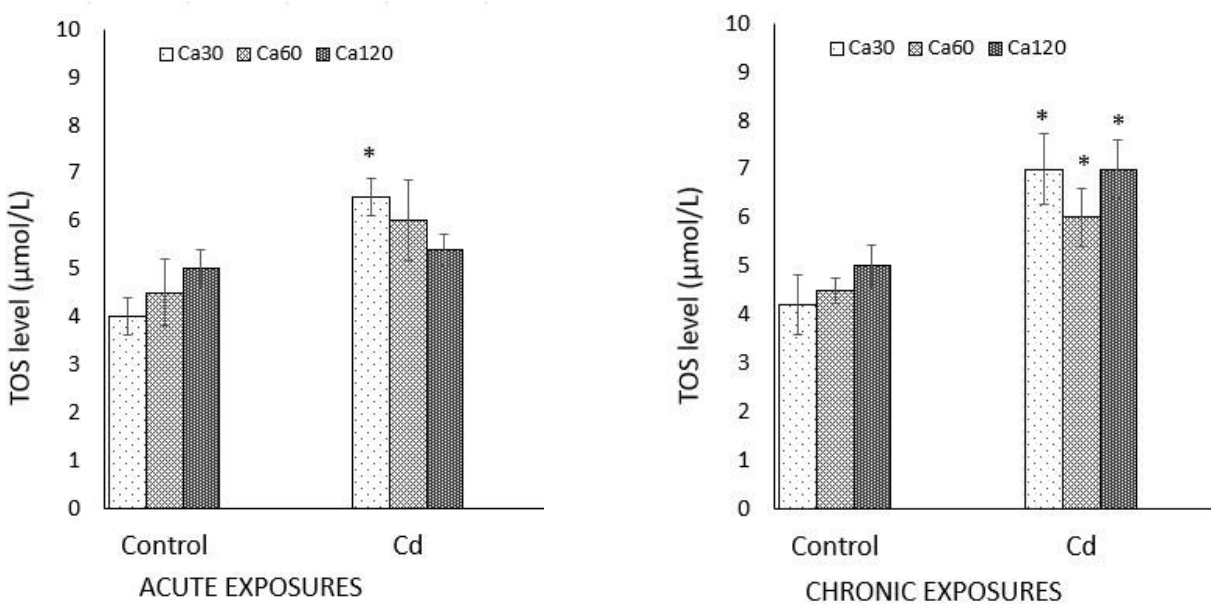

(A) (B)

Figure 1. Total oxidant levels (mean±se) in the serum of fish (*O. niloticus*) exposed to cadmium in differing calcium levels after acute (A) and chronic (B) exposures. Asterisks indicate significant ($p<0.05$) differences between controls and associated cadmium exposures

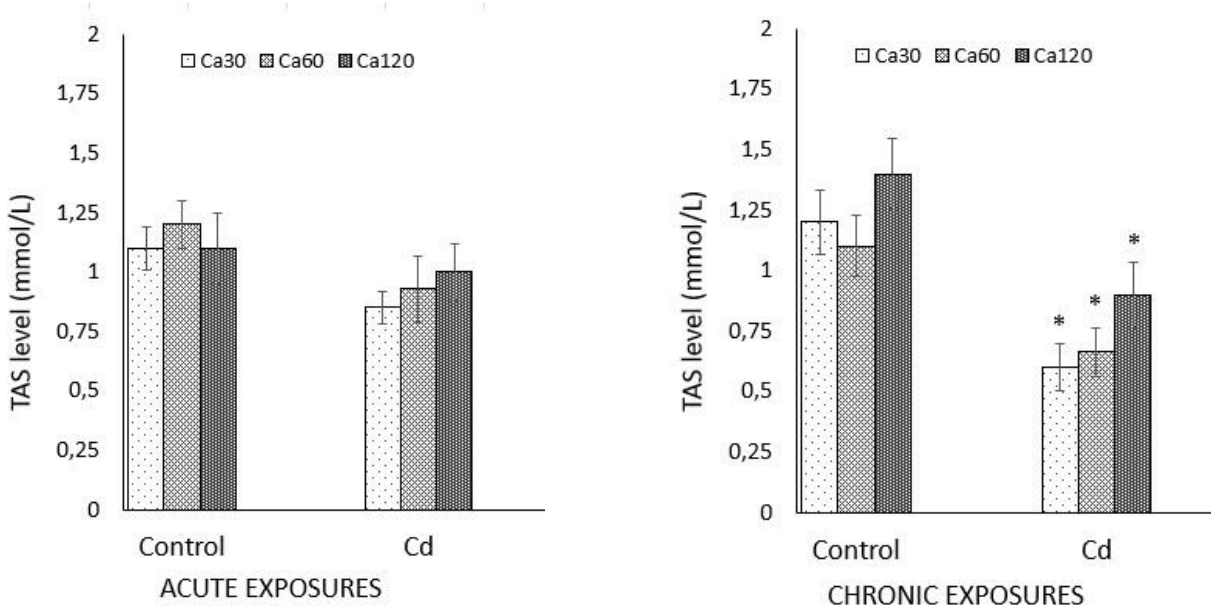

(A) (B)

Figure 2. Total antioxidant levels (mean±se) in the serum of fish (*O. niloticus*) exposed to cadmium in differing calcium levels after acute (A) and chronic (B) exposures. Asterisks indicate significant ($p<0.05$) differences between controls and associated cadmium exposures

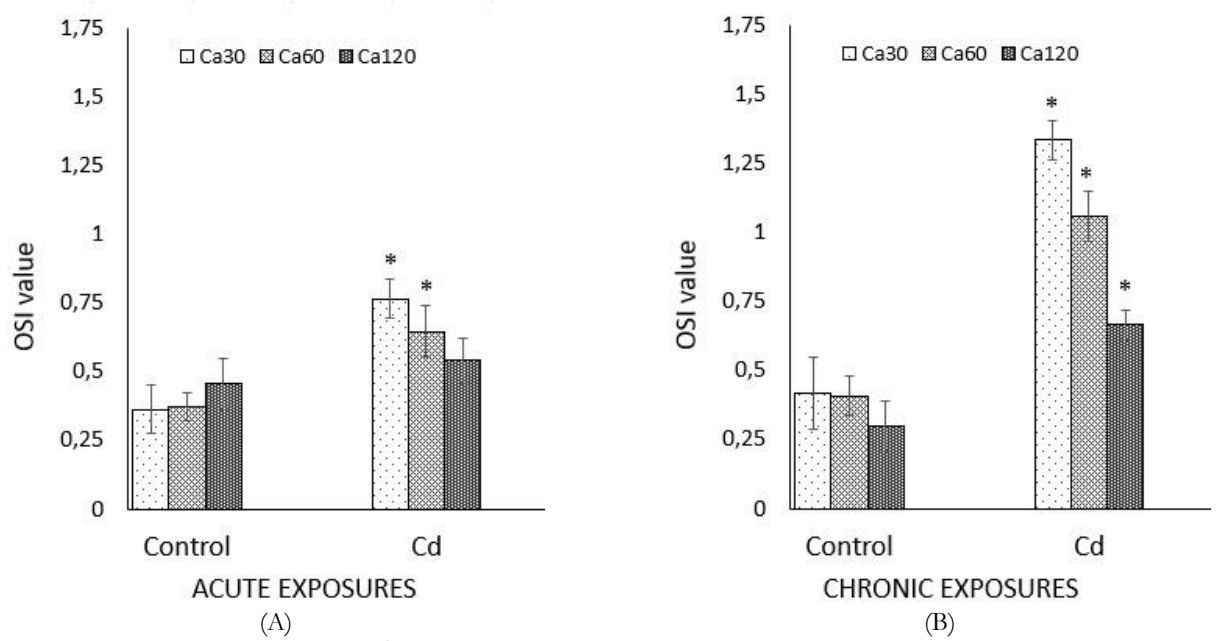

Figure 3. Oxidative status Index values (mean±se) in the serum of fish (*O. niloticus*) exposed to cadmium in differing calcium levels after acute (A) and chronic (B) exposures. Asterisks indicate significant ($p<0.05$) differences between controls and associated cadmium exposures.

3. Results and Discussion

There were no fish deaths after acute and chronic Cd exposures at any calcium level. Likewise, fish did not show any symptoms of appetite loss or abnormality in swimming. This indicates that the exposure conditions and the levels of Cd were not too high and relevant to the environmental situations. The Nile tilapia is known for its tolerance and therefore they are accepted as a good species to study toxicology. This suitability is possibly due to their adaptive capacity to different waters or strong osmoregulation systems to different waters with different chemical qualities [14,15]. In the present study, the results of the measurements showed that TAS levels in the serum of O. niloticus decreased significantly ($p<0.05$) in chronic exposures, though there was no significant change ($p>0.05$) in acute exposures (Figure 1). Oppositely, data showed that TOS levels in the serum of fish increased significantly ($p<0.05$) in both acute and chronic exposures (Figure 2). The changes in TAS and TOS levels also altered the OSI values, as there were significant increases ($p<0.05$) in OSI values in both acute and chronic exposures (Figure 3). When data were investigated in terms of calcium levels, it can be seen that the most significant alterations occurred at the lower calcium levels, emphasizing the protective roles of calcium against Cd toxicity. Nevertheless, the levels of TAS, TOS or OSI did not differ significantly ($p>0.05$) among controls (Ca_{30}, Ca_{60} Ca_{120}), suggesting calcium in water does not have predominant effects on these parameters.

There are considerable amounts of literature data regarding the toxic effects of metals in freshwater fish. Metals seem to affect many physiological metabolisms in fish, changing their activities or levels [1,2,4]. Literature data and our previous studies also showed that metals, including Cd, had toxic effects in different systems of *O. niloticus* such as the antioxidant and osmoregulation systems [16-24]. The above literature data generally demonstrated that chemical or physical qualities of exposure waters such as hardness, salinity and temperature also play direct roles in metal toxicity. Likewise, one of our previous studies also demonstrated that the toxic effects of Cu were more evident in waters with lower conductivity values [25]. In freshwaters, the conductivity levels mainly depend on water calcium levels. Therefore, the authors suggested that environmental monitoring studies in freshwater should the conductivity levels to take into account for meaningful comparison. Because the aquatic systems are generally the final stops of most contaminants discharged by man-made activities, they must be checked often for their metal contaminations. Cadmium is a nonessential metal with no known biological metabolisms and occurs in the environment as a result of anthropogenic activities or from natural sources. After discharge to the aquatic environment, Cd can be accumulated by fish, exerting adverse effects on different metabolisms. Studies also showed that Cd can cause haematological effects, impaired Ca homeostasis, histological and morphological deformation [26-28]. Hazardous effects of Cd in ion-regulating tissues (e.g. kidney, gills and intestine) can lead imbalance of ion concentration in extracellular fluid and an alteration of the osmoregulatory capacity of fish [4,29]. All kinds of toxic effects of metals in different metabolic systems eventually can cause oxidative stress in fish

4. Conclusion

The present data showed that Cd exposures cause an increase in TOS levels and a decrease in TAS levels, affecting OSI values in both acute and chronic durations. However, calcium alone (controls) did not cause any significant change in studied parameters, though calcium played significant roles in the toxic effects of Cd. In this context, data suggested that the toxic effects of metal may be much higher in soft waters compared to hard waters and thus, water hardness levels should be taken into account in environmental monitoring studies.

Acknowledgment (optional)

The author thanks Dr. E.G. Canli for the help during the experiments.

References

[1] Wood, C.M., Farrel, A.P., Brauner, C.J. (2012a). Homeostasis and toxicology of essential metals. Fish. Physiology 31A. Academic Press,, London, p. 497.
[2] Wood, C.M., Farrel, A.P., Brauner, C.J. (2012b). Homeostasis and toxicology of non-essential metals. Fish. Physiology 31B. Academic Press, London, p. 507.
[3] Mance, G. (1987). Pollution threat of heavy metals in aquatic environment. Elsevier, London, 363 pp.
[4] Heath, A.G. (1995). Water Pollution and Fish Physiology, 2nd Edition. New York, NY, USA: CRC Press.
[5] Jorgensen, S.W. (2010). A derivative of encyclopedia of ecology. Ecotoxicology, London, Academic Press.
[6] Priya, K.K., Ramesh, M., Saravanan, M., Ponpandian, N. (2015). Ecological risk assessment of silicon dioxide nanoparticles in a freshwater fish Labeo rohita: Hematology, ionoregulation and gill Na+/K+ ATPase activity. Ecotoxicology and Environmental Safety 120, 295–302.
[7] Ruiz, P., Katsumiti, A., Nieto, J.A., Bori, J., Jimeno-Romero, A., Reip, P., Cajaraville, M.P. (2015). Short-term effects on antioxidant enzymes and long-term genotoxic and carcinogenic potential of CuO nanoparticles compared to bulk CuO and ionic copper in mussels Mytilus galloprovincialis. Marine Environmental Research 111, 107-120.
[8] Zhou, L., Li, M., Zhong, Z., Chen, H., Wang, X., Wang, M., Li, C. (2021). Biochemical and metabolic responses of the deep-sea mussel Bathymodiolus platifrons to cadmium and copper exposure. Aquatic Toxicology 236, 105845.
[9] Canli, E.G. (2022). Farklı Sürelerde Bakır Etkisinde Kalan Tatlısu Midyelerinde (Unio tigridis) Antioksidan Enzim Tepkilerinin Incelenmesi. Kahramanmaras Sütcü Imam Üniversitesi Tarim ve Doga Dergisi 25(1), 31-41.
[10] Uckun, A. A., Uckun, M. (2021). Evaluation of some biomarkers in carp (Cyprinus carpio linnaeus, 1758) depending on water and sediment pollution of Atatürk dam lake. Bitlis Eren Üniversitesi Fen Bilimleri Dergisi, 10(3), 744-753.
[11] Aytekin, T. (2022). Evaluation of the Effects of Nitrilotriacetic Acid as a Chelating Agent on the Biochemical Toxicity of Lead in Oreochromis niloticus. Biological Trace Element Research, 200(6), 2908-2914.
[12] Erel, O. (2004). A novel automated method to measure total antioxidant response against potent free radical reactions. Clinical Biochem. 37(2): 112-119.
[13] Erel, O. (2005). A new automated colorimetric method for measuring total oxidant status Clinical Biochem. 38: 1103–1111.
[14] Cioni, C., Merich, D., Cataldi, E., Cataudella, S., (1991). Fine structure of chloride cells in freshwater-and seawater-adapted Oreochromis niloticus (Linnaeus) and Oreochromis mossambicus (Peters). Journal of Fish Biology 39(2), 197-209.
[15] Kamal, A. H. M. M., Mair, G. C., (2005). Salinity tolerance in superior genotypes of tilapia, Oreochromis niloticus, Oreochromis mossambicus and their hybrids. Aquaculture 247, 189-201.
[16] Oner, M., Atli, G., and Canli, M. (2008). Changes in serum biochemical parameters of freshwater fish Oreochromis niloticus following prolonged metal (Ag, Cd, Cr, Cu, Zn) exposures. Environmental Toxicology and Chemistry, 27: 360–366.
[17] Canli, E.G., Dogan, A., Canli, M., (2018). Serum biomarker levels alter following nanoparticle (Al2O3, CuO, TiO2) exposures in freshwater fish (Oreochromis niloticus). Environmental Toxicology and Pharmacology 62, 181-187.
[18] Kanak, E.G., Dogan, Z., Eroglu, A., Atli, G., Canli, M., (2014). Effects of fish size on the response of antioxidant systems of Oreochromis niloticus following metal exposures. Fish Physiology and Biochemistry 40, 1083-1091.
[19] Atli, G., Yuzbasioglu Ariyurek, S., Kanak, E.G., and Canli, M. (2015). Alterations in the serum biomarkers belonging to different metabolic systems of fish (Oreochromis niloticus) after Cd and Pb exposures. Environmental Toxicology and Pharmacology, 40: 508–515.
[20] Gopi, N., Vijayakumar, S., Thaya, R., Govindarajan, M., Alharbi, N. S., Kadaikunnan, S., Vaseeharan, B. (2019). Chronic exposure of Oreochromis niloticus to sub-lethal copper concentrations: effects on growth, antioxidant, non-enzymatic antioxidant, oxidative stress and non-specific immune responses. Journal of Trace Elements in Medicine and Biology 55, 170-179.
[21] Dogan A, Canli M (2019). Investigations on the osmoregulation system of freshwater fish (Oreochromis niloticus) exposed to mercury in differing salinities. Turkish Journal of Fisheries and Aquatic Sciences 19(12): 1061-1068.

[22] Mohamed, A. A. R., El-Houseiny, W., Abd Elhakeem, E. M., Ebraheim, L. L., Ahmed, A. I., Abd El-Hakim, Y. M. (2020). Effect of hexavalent chromium exposure on the liver and kidney tissues related to the expression of CYP450 and GST genes of Oreochromis niloticus fish: Role of curcumin supplemented diet. Ecotoxicology and Environmental Safety 188, 109890.
[23] Hossain, Z., Hossain, M. S., Ema, N. S., Omri, A. (2021). Heavy metal toxicity in Buriganga River alters the immunology of Nile tilapia (Oreochromis niloticus L). Heliyon 7(11), e08285.
[24] Karayakar, F., Yurt, Ö., Cicik, B., Canli, M. (2022). Accumulation and elimination of cadmium by the nile tilapia (Oreochromis niloticus) in differing temperatures and responses of oxidative stress biomarkers. Bulletin of Environmental Contamination and Toxicology 109 (6), 1126-1134.
[25] Canli, E. G., Canli, M. (2015). Low water conductivity increases the effects of copper on the serum parameters in fish (Oreochromis niloticus). Environmental Toxicology and Pharmacology, 39(2), 606-613.
[26] Monserrat, J.M., Martinez, P.E., Geracitano, L.A., Amado, L.L., Martins, C.M.G., Pinho, G.L.L., Chaves, I.S., Ferreira-Cravo, M., Ventura-Lima, J. and Bianchini, A. (2007). Pollution biomarkers in estuarine animals: Critical review and new perspectives. Comparative Biochemistry and Physiology, 146C: 221-234.
[27] Ezemonye, L.I.N. and Enuneku, A.A. (2011). Biochemical alretaions in Hoplobatrachus occipitalis exposed to sublethal concentrations of cadmium. Turkish Journal of Fisheries and Aquatic Sciences, 11: 485-489.
[28] Besirovic, H., Alic, A., Prasovic, S. and Drommer, W. (2010). Histopathological effects of chronic exposure to cadmium and zinc on kidneys and gills of brown trout (Salmo trutta m. fario). Turkish Journal of Fisheries and Aquatic Sciences, 10: 255-262.
[29] McGeer, J.C., Szebedinszky, C., McDonald, D.G., and Wood, C.M. (2000). Effects of chronic sublethal exposure to waterborne Cu, Cd or Zn in rainbow trout. 1: Iono-regulatory disturbance and metabolic costs. Aquatic Toxicology, 50: 231–243.

Cukurova University
Journal of
Natural & Applied Sciences

Original Paper

Historical Background of Polymeric Optical Fibers and Woven Fabrics Made of POFs

Can Esmercan[1], Füsun Doba Kadem[1]

[1]Department of Textile Engineering, Çukurova Üniversitesi, Türkiye

ORCID IDs of the authors: C.E. 0009-0007-6826-4415; F.D.K. 0000-0002-7764-5910

Cite this article as: Esmercan C., Kadem F.D. (2024). Historical Background of Polymeric Optical Fibers and Woven Fabrics Made of POFs. Cukurova University Journal of Natural & Applied Sciences 3(1): 25-31.

Abstract

Polymeric optical fibers (POF) are mono-filaments that guide light and are primarily used for transmitting data over short distances, as well as for fiber-optic sensors and illumination purposes. These fibers are composed of polymers. Fiber production is inexpensive compared to glass fibers, and the products are more long-lasting than glass optical fibers (GOF). POFs can be classified into step-index fibers (SI-POF) and graded index profile fibers (GI-POF) based on their index profile. At first, only fibers with step-index were manufactured. The need for an augmentation in the potential data transmission rates has resulted in the creation of an index profile, GI-POF. POF materials are appropriate for transmitting data over short distances and can be integrated with textile structures. Because short-distance data transfer is sufficient when using POFs in textile structures, SI-POF is a more viable option than GI-POF due to its lower production cost and the required data transfer distance. The primary goal of incorporating POF material into textile fabrics is to facilitate media transmission, such as light. POFs can be readily incorporated into a fabric by weaving. The historical context of the production of POF in a step-index profile and the process of weaving POF has been extensively studied in the literature.

Keywords: Polymeric optic fiber, POF, SI-POF, weaving, woven, fabric

1. Introduction

Polymeric optical fibers (POF) are single filaments that guide light and are primarily used for transmitting data over short distances, as well as for fiber-optic sensors and illumination purposes. POF generally consists of circular fibers with a core-cladding structure. The core of the optical fiber is responsible for transmitting light. At the same time, the cladding is necessary to create a reflective interface with a consistent ratio of refractive indices, enabling total internal reflection.

POFs are used for data transmission, require extraordinary optical quality, and are produced using a highly specialized process. Regarding textile illumination using POF fabrics, the optical requirements for the POF are lesser significance. Nevertheless, the cost becomes crucial because of the substantial amount of POF needed for illumination [1]. Figure 1 displays the POF with woven fabric in the use of textile illumination.

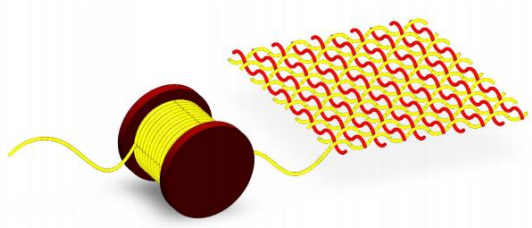

Figure 1. POF with woven fabric for textile illumination [1]

Address for Correspondence:
Can Esmercan, e-mail: cesmercann@gmail.com

Received: Jan 26, 2024
Accepted: Apr 22, 2024

The predominant focus of POF literature revolves around communication. The uses of POFs go beyond data transmission. The illumination industry is one of the largest markets. POF is ideally suitable for integration into textiles. Several fabrics are comprised of POFs. Subsequently, these fibers can be employed for lighting, wearable sensors, or communication.

POFs with a pure step-index profile, also known as SI-POF, were the initial fibers developed. This implies that a straightforward optical cladding encompasses a uniform core. The routes within the fiber are determined similarly to a ray in geometric optics. Using step-index fibers, the ray's path is traced until it reaches the core interface and cladding interface. At this point, the ray's reflection is considered by recalculating the direction of propagation. When the reflection is optimal, the angle of incidence and the angle of reflection are identical. Over the past few years, there has been a significant emphasis on examining and advancing smart or intelligent textiles. As part of the intelligent textile category, POF textiles have attracted significant attention due to their pliability, lightweight nature, resistance to electromagnetic interference (EMI), ease of manipulation, straightforward connectivity, and compatibility with living organisms. POF can be integrated into textile structures by different techniques such as weaving, knitting and braiding [1].

The main objective of integrating POF into textiles is to facilitate light transmission. Light can illuminate fibers indivudually to achieve practical effects in fabrics, such as creating a pleasant atmosphere or enhancing safety in sports textiles. Light can be conveyed over long distances by travelling along an uncurved trajectory. Nevertheless, due to the phenomenon of refraction, the luminous power decreases over shorter distances when transmitted through undulating or looped structures. In order to take advantage of the benefits of POF material, the illuminated yarns within a fabric need minimal undulation or to be straight. Textiles can be produced from yarns with minimal undulation by weaving or braiding techniques. Both warp and weft knitting methods generate loop formation. They are susceptible to bending and mechanical strain. Weaving is the most widely regarded textile technique for transforming optical fibers into textile formations [1]. Figure 2 displays the luminous intensity of POFs depending on their different bent yarn paths.

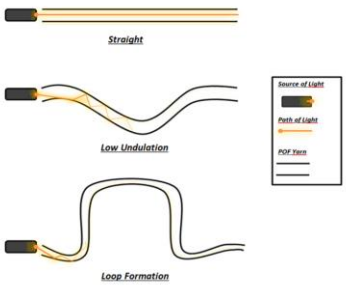

Figure 2. Diminution of luminous intensity resulting from refraction in differently bent yarn paths [2]

Since the 19th century, the production of POF has been initiated for industries. Initially, POF manufacturing was primarily used for data transmission, but it later expanded to include textile applications. SI-POFs are commonly employed in textile applications due to their limited data transmission range and reduced manufacturing expenses. In addition, during the 19th century, textile fabrics made from POF were manufactured for illuminating applications. These manuscripts are intended to demonstrate the historical background of both POF production and POF woven fabric to guide future trials and research.

2. Literature Review

2.1. Literature Review of Polymeric Optic Fibers

In the latter half of the 19th century, there was significant research interest in the idea of illuminating glass rods. This was because dentists needed technologies that could guide light to illuminate the entire mouth, as well as for other medical purposes such as imaging, spectroscopy, endoscopy, tissue pathology, blood flow monitoring, light therapy, biosensing, biostimulation, laser surgery, dentistry, dermatology, and health status monitoring. Optical fibers were first used in medicine to provide internal illumination during endoscopic procedures. In 1965, Manfred Borner developed the inaugural optical-data transmission system utilizing optical fibers at the Telefunken Research Laboratories in Ulm, Germany. The technology was granted a patent in 1966. Theodore Maiman's invention of the first laser system in 1960 marked a significant technological breakthrough [2,3].

The emergence of laser technology is the starting point for the development of long-distance operational glass fibers and POF. In the late 1960s, research on light-guiding fibers diverged into two branches: glass and polymer-based optical fibers, which had just been developed. During the latter decades of the 20th century and the early years of the 21st century, significant advancements in fabrication technology have led to a substantial reduction in fiber losses. POF applications are well-suited for data transfer, sensor technology, and the integration of fibers into functional textiles. These applications have significant market potential. The value of previously published works on POF is attributed mainly to the innovative features of current material selections, intelligent fabrics, and the market review [2].

Because the monomer materials used were not pure enough, the attenuation remained at approximately 1.000 dB/km. During the 1970s, it significantly reduced losses, approaching the theoretical limit of approximately 125 dB/km at wavelengths of 650 nm. During that period, there were ample supplies of glass fibers with shallow losses of less than 1 dB/km at wavelengths of 1,300 nm and 1,550 nm. However, these fibers were only available at a higher cost. Following the complete digitization of data communication for long-distance transmission in the 1990s, significant advancements in digital systems for individual users began. The annual international conference for POFs and applications, held since 1992, is a significant indicator of the advancements made in this specialized field [4].

POF provides substantial benefits compared to glass alternatives. More precisely, the substantial diameter of these connections, typically ranging from 0.25 to 1 mm, allows for the utilization of inexpensive plastic connections with lower levels of accuracy, resulting in a reduction in the overall cost of the system. Furthermore, POF stands out due to its enhanced adaptability, ability to withstand shocks and vibrations, and efficient light transmission from the light source to the fiber. As a result of these advantages, numerous POF applications have been created and commercialized [5].

Table 1. Historical development of the most significant SI-POF landmarks during the past 45 years [1]

Year	Organization	Milestone
1968	Dupont	First SI POF with PMMA core
1972	Toray	First SI POF with PS core
1976	Mitsubishi Rayon	Produced Eska™, a PMMA SI-POF: >300 dB/km @650 nm
1981	NTT	Low attenuation PMMA SI POF 55 dB/km at 568 nm
1982	NTT	First SI POF with deuterated PMMA core 20 dB/km at 650 nm
1983	Mitsubishi Rayon	Produced step-index PMMA-POF: 65 dB/km @570 nm
1991	Hoechst Celanese	SI PMMA "Infolite" POF 130 dB/km at 650 nm.
1993	Essex University	Transmission at 631 Mbps over 100 m by means of a PMMA-core SI POF and an equalizer circuit
1994	Asahi Chemical	First multicore SI POF for high speed transmission
1995	Mitsubishi Rayon,NEC	Transmission at 156 Mbps over 100 m by means of a low NA SI POF and a fast red LED
1997	POF Consortium of Japan	Standardization at ATM LAN 156 Mbps over 50 m of SI POF in the ATM Forum.
1997	POF Consortium of Japan	Standardization of the norm IEEE 1394 156 Mb/s over 50 m of SI POF.
1998		MOST Standard for Automobiles started
2006-2007		10 Mbps over 400 meters of 1 mm SI POF (4-PAM, 8-PAM
2006-2007		100 Mbps over 200 meters of 1 mm SI POF (4-PAM, 8-PAM)
2011	POF-PLUS	1 Gbps over 50 meters of SI PMMA
2011	Opto Marine Co., Ltd. /Korea	1 mm SI POF with data rates of 500 Mbps, 5 Gbps and 10 Gbps at 100 meters at 650 nm.
2013	KDPOF/Spain	1 Gbps of SI POF for Automotive Industry

The progression of SI-POF can be seen in Table 1. The primary focus of POF literature revolves around communication. POFs have a wide range of uses beyond just transmitting data. POF is highly compatible with integration into textiles. Many textiles consist of polymer fibers. Subsequently, these fibers can be employed to provide light, function as sensors that can be worn, or facilitate communication [2].

Digitalization is happening constantly, especially in industrial controls, consumer electronics, and automotive applications that need cheap, short-range connectivity and better performance. This will make the market for POF solid and stable in the future. POF has also capitalized on a vast market with diverse applications. The utilization of GOF primarily focuses on the communications and IT industries, whereas POFs are employed across a wide range of sectors, ensuring minimal risk of downturns. GOF did not penetrate the short-distance market due to its high cost, intricate design, and operating frequency. POF has a significant opportunity due to reduced prices, improved performance, and resistance to electromagnetic noise and interference [2].

2.2. Literature Review of Polymeric Optic Fiber Woven Fabrics

Weaving is the predominant technique for producing POF textile structures, surpassing the usage of knitting and embroidery methods. Incorporating POF into woven structures is essential for attaining a luminance effect. This can be accomplished by minimizing the bending of POF at a considerable [6].

The incorporation of POF into woven fabrics was first documented in the early 1960s. POFs are commonly used in weaving as weft yarns. Indeed, they can also be employed as warp yarns. This is typically the case for ribbon fabrics, as they are incredibly narrow. Standard multifilament or staple fiber yarns composed of cotton, PET, or other materials can be utilized for the second thread. Transparent yarns enhance the evenness of luminance by allowing the radial light emitted from the POF beneath them to pass through [7].

Before implementing beam warping, defining the application of POF is necessary. It has a great importance to know in which application POFs will be used. According to the application, also desired précised bending and illumaniton effects could be considered to use POFs as warp or weft POF used as weft yarn exhibits greater versatility compared to POF used as warp yarn. Predefining the patterning is unnecessary. Nevertheless, not all methods of inserting weft are suitable for processing POF [2].

In 1979, Maurice Daniel conducted research to develop a fabric that incorporates fiber optic illumination, with the fiber optic elements integrated into the fabric's threads. Another aim of this invention is to present a technique for illuminating apparel using fiber optic technology. The previous invention aimed to incorporate POF into a textile product in order to illuminate and display the light-transmitting section of the POF in relation to the textile product. However, the primary objective of this study was to demonstrate the consistency of illumination. The invention involved integrating POF as a substitute for traditional fabric yarns, such as warp and weft. The invention claimed to incorporate fiber optics into the fabric, enabling their use for purposes such as illumination, heat, or suntanning [8].

In 1988, Jeffery R. Parker conducted a study on enhancing the optical efficiency of a light-emitting panel and increasing its light output. Typically, when light enters one end of POF, it emerges from the other end but decreases the intensity. Nevertheless, light will be emitted at these locations if the surface of the optical fiber is scratched or deformed due to bending at specific points. The panel is optimally designed to serve as a backlight for a liquid crystal or similar device. It efficiently transmits light to the emitter surface from a distant light source through a cable or light conduit connected to either or both ends of the emitter surface [9].

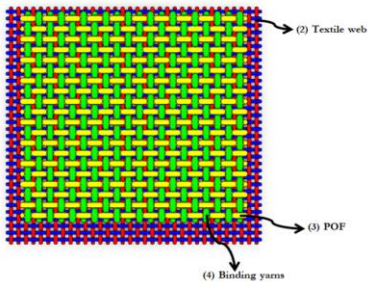

Figure 3. Textile web and POF [4]

Delphine Molhamme conducted a study in 2007 on a fabric web that consists of optical fibers woven with binding yarns. These optical fibers can emit light sideways. The illuminating assembly comprises a textile web (2) in which POF(3) is interwoven with binding yarns (4). The binding yarns (4) arrangement typically follows the warp direction, while the POF (3) is typically arranged in the weft direction, depending on the specific implementation. In order to improve the lighting properties of an illuminating structure that consists of a textile web (2), it is possible to locally weave binding yarns (4) with POF(3). The binding yarns, when interwoven in a "fabric" weave, can create empty spaces that enable the transmission of the optical fibers' luminous energy. The textile web is affixed to a rigid substrate and adhered using a bonding agent. POF (3) maintains constant communication with bonding intermediate in this scenario. The bonding intermediate facilitates the direct reflection of light emitted by POF. Figure 3 displays the presence of the textile web and POF [10].

The interior of the optical fibers can be made of one of the following materials: polymethyl-methacrylate (PMMA), polycarbonate (PC), or Cyclo-Olefin Polymers (COP). The yarns used for binding were woven from synthetic fibers.

In 2013, Thomas Franz et al. studied an illuminated fabric composed of glass fibers. The invention aims to create a radiant textile that exhibits exceptional lighting capabilities and maintains consistent brightness throughout its entire surface. Glass is a highly transparent substance to visible light. Utilizing glass fibers prevents light attenuation in the luminous woven fabric, thereby enhancing its optical efficiency and luminosity. The research shows that the luminous woven fabric is made up of glass yarns with a tex of 68 as the warp yarns and POF produced from PMMA/PTFE with a diameter ranging from 250 µm to 500 µm as the weft yarns. This combination of materials makes for good lighting levels. The woven textile supports are created using a 4, 8, and 12 harness satin weave, with a weft density ranging from 8 to 14 yarns per centimeter. The best lighting happens when optical fibers are 500 µm in diameter and have a density of at least 8 yarns/cm, preferably at least 10 yarns/cm, and ideally at least 12 yarns/cm are used in woven textile supports. Using specific-sized glass filaments as warp yarns increases the chances of increasing the density of optical fibers [11].

Also, in 2013, Hans-Joachim Kobek researched to develop a textile fabric with consistent luminosity throughout. The self-luminous fabric, which is already known, includes an additional layer of transparent yarns positioned directly above the second layer. This layer functions as a diffuser, dispersing light evenly. Given its established arrangement, the objective is to achieve consistent illumination across the entire surface of the self-luminous fabric. Controlling this configuration of either transparent or partially transparent fibers is challenging and relies on the specific type of light coupling. The luminosity of the light-emitting surface is insufficient due to the omnidirectional emission of light from the light-emitting yarns, which lack a specific direction of light emission. Currently, no structure can separate the emitted light in a way that allows it to be directed with a high level of brightness and a consistent brightness perception on the side where the light is emitted. The objective is accomplished by implementing a light decoupling structure where reflector elements are printed on at least one side of the luminescent textile's surface. These reflector elements are specifically designed to reflect light in a targeted manner and thus adhere to the light-guiding elements. This fabric utilizes the POF. One side of the luminescent textile contains flexible reflector elements that are distributed and bonded to the surface of the threads in a coating process. These reflector elements maintain the flexibility of the textile and are designed to reflect the light emitted into the fibers. Figure 4 displays the weft yarn as POF(1), the warp yarn(2), the reflector elements (10), and the crossing point of the weft and warp yarns (30). The invention primarily involves the creation of a uniformly bright and consistent surface [12].

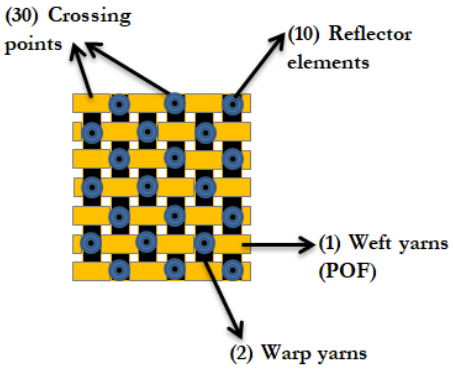

Figure 4. Fabric with reflector elements [12]

Zhou Leijing studied a flexible light-guiding optical fiber fabric in 2014 at Ningbo Jingzhi Electronic Technology Co. in Shenzhen, Guangdong, China. The invention uses a pliable fabric made of optical fibers that transmit light. The weft threads are formed by alternating PMMA optical fibers, while the warp threads consist of regular yarns. The diameter of the POF ranges from 0.2 mm to 0.8 mm. This fabric uses a sateen weave with 8 or 16 picks in the weft direction. The claims aspect of the application involves utilizing the flexible light-conducting POF fabric in domestic textiles and dress ornaments [13].

The comprehensive Table 2, which pertains to the information below regarding their region, active timespan, status, etc., is displayed.

Table 2. Historical background of weaving [14]

Year	Inventors	Main Claim	Landscape	Timespan	Status	Assignee
1967	Burton N.Derick	Luminous textile products	Delaware, ,USA	1967-1987	Expired	EIDP Ltd.
1979	Maurice Daniel	Fabric with fiber optic illumination	Ohio, USA	1979-1999	Expired	Individual
1988	Jeffrey R. Parker	Improve the optical efficiency of a light emitting panel	Ohio, USA	1988-2008	Expired	Lumitex Inc.
2007	Delphine Malhomme	Fabric web comprising warp and/or weft optical fibers	Villeurbanne,FR	2007-2009	Abandoned	Brochier Technologies
2013	Thomas Franz	Illuminated fabric which comprising glass fibers	Chambery,FR	2013-2016	Abandoned	Saint Gobain Adfors SAS
2013	Hans-Joachim Kobek	Uniformly luminous textile fabric	Traunreut, DE	2013-	Active	Motherson Innovations Lights GmbH
2014	Zhou Leijing	Flexible light-guiding optical fiber fabric	Guangdong,CN	2014-	Pending	Ningbo Jingzhi Electronic Technology Co. Ltd.
2015	Leng Jianjun Zhang Fang	Polymeric optical fiber, luminous fabric and its manufacture method	Jiangsu,CN	2015-	Active	Xuzhou Guohong Packaging Co., Ltd
2021	Benjamin Mohr Niklas Stracke	Device and method for preparing a fiber optic fabric	Bochum, DE	2021	Active	Munda Textile Lichtsysteme GmbH

In 2015, Leng Jianjun researched POF and luminous fabrics in Jiangsu, China. This undertaking produces luminous fabrics by intertwining weft yarns as POF. The POF within the fabric undergoes weaving on the loom, and the POF, after being bound and connected to a specific light source, creates a luminous POF fabric. The warp thread consists of man-made fibers with a line density ranging from 120 to 300 tex. The weft yarn is made of POF, and the light source is a 5 mm blue LED. The fabric possesses the subsequent attributes: The weft density and thickness are 250 per 10 cm. Due to the intricate weaving of POF, it possesses high durability, and the resulting luminous fabric exhibits exceptional brightness and longevity [15].

In 2021, Benjamin Mohr and Niklas Stracke conducted research on a device and technique for fabricating a fiber optic fabric. The objective of this invention is to offer a device and technique that allows for the preparation of a fiber optic fabric in the most straightforward and adaptable manner, enabling efficient, flexible, and controlled introduction of light into the fabric. The length of the exposed ends of the light-guiding fibers can vary across the width of the light-guiding fabric. The device based on the invention offers a notable benefit in that the level of exposure of the ends of the light-conducting fibers can be determined separately from the fabric. This determination can be achieved through the design of the combing device or by adjusting the relative movement of the combing element and the feed device [16].

3. Results and Discussion

The production of SI-POF has made significant advancements in reducing attenuation over the past 45 years. The advancement and tangible outcomes of POF manufacturing have generated significant prospects for textile lighting applications. The utilization of POF in textile illumination applications has yielded favourable outcomes, showcasing the weaving capabilities of POF through numerous examples. These trials have been conducted using various weaving patterns and methods to incorporate POF into woven textiles for illuminating textile applications.

4. Conclusion

POFs are utilized for both illumination purposes and data transmission. These enlightening applications are seamlessly incorporated into textile structures. POFs are required to exhibit reduced bending in order to facilitate their integration into textiles, as there is a risk of POFs breaking. POF for data-transmission must have a very high optical quality and are therefore manufactured through a very specialized procedure. When it comes to textile illumination with POF fabrics, the optical criteria for the POF are less important. In addition to the production of fibres, weaving is vital for the textile illumination. POFs are most effectively incorporated into textiles through the process of weaving. This manuscript serves as a guide by presenting the production and advancement of POF, a material that has experienced significant growth in recent years. It also discusses the incorporation of POFs into textile applications and the latest weaving applications of POFs for upcoming research and experimentation.

Acknowledgment

This study is a part of master thesis carried out with the project titled FYL-2022-15607 'Polimerik Optik Fiberler ile Dokunan Kumaşların Dokumadaki Bükülme Yapısına Göre Analizi (Analysis of POF Woven Fabric With Respect to Their Bending) and it is supported by Çukurova University Scientific Research Projects Unit.

References

[1] Esmercan C., (2024). Analysis of Polymeric Optical Fibers (POF) Woven Fabrics with Respect to Bending. Çukurova University Master Thesis. Adana.

[2] Bunge C.-A., Beckers M. ,Gries T. (2017). Polymer Optical fibers fiber Types, Materials, Fabrication, Characterisation and Applications. United Kingdom. https://doi.org/10.1016/C2014-0-00562-X.

[3] Gang-Ding P. (2019). Handbook of Optical fibers. Sydney, NSW, Australia. https://doi.org/10.1007/978-981-10-7087-7.

[4] Krauser J., Ziemann O., Zamzow P.E., Daum W., (2007). POF Handbook. Berlin,DE. DOI 10.1007/978-3-540-76629-2.

[5] Arrue J., Zubia J.(2001). Plastic Optical Fibers: An Introduction to Their Technological Processes and Applications. 100-101. doi:10.1006 ofte.2000.0355.

[6] Ge L. (2021). Novel Woven Structure Design for Polymeric Optical fiber (POF) Textiles. PhD report. Institute of Textiles and Clothing, The Hong Kong Polytechnic University, Hung Hom, Hong Kong.

[7] Kallweit J., Pätzel M., Pursche F., Jabban J., Morobeid M., Gries T. (2021). An Overview on Methods for Producing Side-Emitting Polymer Optical fibers. 337–360. https://doi.org/10.3390/ textiles1020017.

[8] Daniel M. (1979). Light emitting fabric. Google patents: US4234907.

[9] Parker J.R. (1988). fiber optic light emitting panel and method of making same. Google patent: US4885663.

[10] Brochie C., Malhomme D., Deflin E. (2006). Illuminating complex comprising a light source having a web of optical fibers. Google patents: US20090291606A1.

[11] Franz T., Fasching J., Mikulecky B., Wandji N.O., Jacquiod C., Espiard P., (2013). Illuminated fabric comprising glass fibers. Google Patent: US20160122911A.

[12] Kobek H.-J. (2013). Uniformly luminous textile fabric. Google patent: DE102013020715B4.

[13] Leijing Z. (2014). Flexible light-guiding optical fiber fabric. Google patent: CN104164734A.

[14] Esmercan C., (2023). Analysis of melt-spun POF woven fabric. RWTH Aachen master project report. Aachen.

[15] Jianjun L., Fang Z. (2015). Polymer optical fiber, luminous fabric and its manufacture method for luminous fabric, Google patent: CN105133084B.

[16] Mohr B., Stracke N. (2021). Device and method for preparing a fiber optic fabric. Google patent: DE102021109194B4.

Cukurova University
Journal of
Natural & Applied Sciences

Original Paper

Development of Cargo Delivery Time Prediction Models

Selim Hanedar[1], Ceren Ulus[2], M. Fatih Akay[2]

[1]Trendyol, Department of Technology, İstanbul, Turkey
[2]Çukurova University, Department of Computer Engineering, Adana, Turkey

ORCID IDs of the authors: S.H. 0009-0004-7037-1840; C.U. 0000-0003-2086-6381; M.F.A. 0000-0003-0780-0679.

Cite this article as: Hanedar, S., Ulus, C., Akay, F.A. (2024). Development of Cargo Delivery Time Prediction Models, Cukurova University Journal of Natural & Applied Sciences 3(1): 31-35.

Abstract

E-commerce stands out as the sales form with the fastest growth momentum with high sales volumes. Managing sales volumes efficiently is of great importance in maximizing customer satisfaction. By accurately predicting delivery times, effec-tive logistics optimization is achieved and customers are informed about how long it will take for their cargo to be delivered. In this study, it is aimed to develop cargo delivery time prediction models with machine learning-based Categorical Boosting (CatBoost), Decision Tree (DT), Extreme Learning Machine (ELM), Light Gradient Boosting Machine (LightGBM) and Support Vector Machine (SVM). The 5113-row dataset contains delivery history information for the 16-month period between February 14, 2019, and June 13, 2020. The performance of the developed models has been evaluated using Mean Absolute Percentage Error (MAPE) by utilizing 5-fold cross-validation on the dataset. The results show that the models developed using SVM exhibited the most successful prediction performance.

Keywords: Delivery Time Prediction, Machine Learning, E-Commerce

1. Introduction

E-commerce is attracting attention as a fast-growing sector and is causing radical changes in the world of commerce. In the first half of 2023, the share of trade in total trade increased to 19.1%, which illustrates the growth potential of the sector [1]. In this context, the development of e-commerce offers small and medium-sized enterprises the opportunity to compete and grow in global markets. Establishing themselves in this highly competitive market allows companies to expand their cus-tomer base, increase their market share, strengthen brand awareness and improve the customer experience through continu-ous innovation. However, to thrive in the highly competitive e-commerce environment, customer satisfaction must be max-imized. Providing a user-friendly website, solution-oriented customer service and fast and reliable delivery are strategic measures that increase customer satisfaction.

In recent years, fast delivery has become increasingly important in the modern e-commerce world as customer expectations shift towards instant gratification, offering competitive advantages and increasing customer satisfaction. The proliferation of services such as Amazon Prime, Hepsiburada and Trendyol has enabled consumers to view fast delivery as the norm. Busi-nesses that offer fast delivery can stand out in a competitive market, expand their customer base and build a loyal customer base. The combination of these factors has led to fast delivery, which is becoming an essential element in the e-commerce industry [2].

Research shows that customer satisfaction is 20-30 higher for companies that offer fast delivery than others. In addition, it has been observed that the likelihood of customers making repeat purchases increases by up to 70% for companies that offer fast delivery. It has been determined that companies with customer profiles that share their fast delivery experiences on social media have lower complaint and return rates than other companies [3].

Cargo companies focus on basic components such as shortening delivery times, reducing costs, and delivering products to customers without damage. These components are evaluated using data received from cargo companies and are reflected in agreements made with parameters such as regional deadlines and the number of packages for regional and non-regional de-liveries. Although these standards are shaped within a certain framework, differences in delivery times may occur due to the product diversity and customer profile of each brand. These differences are of great importance as they can cause the loss of potential

Address for Correspondence:
Ceren Ulus, e-mail: f.cerenulus@gmail.com

Received: May 24, 2024
Accepted: June 3, 2024

customers. To overcome these differences, brands must constantly optimize their logistics processes, increase operational efficiency, and provide flexibility to quickly respond to customer demands.

In this context, delivery time estimation stands out as a strategic tool that enables the optimization of logistics processes. This study aims to predict delivery time using machine learning-based methods. For this purpose, prediction models have been developed using CatBoost, DT, ELM, LightGBM and SVM.

This study is organized as follows: Section 2 includes relevant literature. Methodology is presented in Section 3. Section 4 presents delivery time prediction models. Results and discussion are given in Section 5. Section 6 concludes the paper.

2. Literature Review

[4] presented the Marine Predators Algorithm (MPA) for Shipment Status Time Prediction (STP). Initially validated on nu-merical benchmark problems, STPMPA surpassed all algorithms, demonstrating superior performance. Employing Extreme GB optimizers, STPMPA outperformed compared optimization algorithms for the STP problem, illustrating its efficacy in producing efficient forecasts for real-time systems. [5] proposed the Heterogeneous HyperGraph Neural Network (H2GNN) model for estimating package arrival time. This model introduced an order heterogeneous hypergraph, where hyperedges represent orders and nodes represent order attributes. Leveraging Hyper-Graphsage, H2GNN extended hypergraph learning to large-scale e-commerce data, enabling informative representations of packages by preserving both structure-based infor-mation learned by hypergraph and feature-based information captured by Transformer, ultimately outperforming baseline methods. [6] introduced the Knowledge Distillation Graph (KDG) NN based package Estimated Time Arrival (ETA) pre-diction model, termed KDG-ETA. This model utilized information densification to condense past trip knowledge into Origin-Destination pair embeddings, thereby combining context embeddings from the feature extraction module with com-prehensive trip information. An adaptived attention module was incorporated for delivery time estimation, resulting in a 3.0% to 39.1% reduction in Mean Absolute Error. [7] proposed Heterogeneous Tasks Aware Package Pick-Up Time (HTAPT), a package pickup time prediction framework comprising a pre-trained arrival time prediction module and a pickup time and route prediction module. HTAPT demonstrated improved forecast accuracy by up to 10% compared to state-of-the-art methods. [8] aimed to develop a novel machine learning forecasting method by integrating time series data features and the Adaptive Neuro-Fuzzy Inference System. Their proposed framework established a four-stage operations model, facilitating systematic forecasting of real-time e-order arrivals at distribution centers to enhance third-party logistics providers' efficiency in handling hourly e-order arrival rates. [9] introduced the Graph Structure Learning-based Quantile Regression (GSL-QR) model for e-commerce ETA prediction. GSL-QR dynamically updated spatial and temporal order relationships using graph structure learning optimized for ETA forecasting tasks. This multi-objective quantile regression model guaran-teed both forecasting accuracy and order fulfillment rate, demonstrating superiority over baseline models. [10] presented the Inductive Graph Transformer (IGT), which leverages raw feature information and structural graph data to estimate package delivery time. IGT's discrete pipeline-trained transformer captured various information from raw features and dense embed-ding data as a regression function, thus outperformed state-of-the-art methods in delivery time prediction. [11] aimed to assess the effectiveness of e-scooter sharing services in the delivery of postal services in Turkey by estimating the delivery time and energy cost of e-scooter vehicles for distributing mail or goods. Random Forest (RF), GB, K-Nearest Neighbor, and NN were among the machine learning algorithms used. They discovered that the GB algorithm had better prediction per-formance for energy cost and delivery time, demonstrating the financial and environmental benefits of e-scooter delivery vehicles over conventional vehicles. [12] developed a data-driven framework for managing customer expectations and im-proving satisfaction. Utilizing tree-based models, their approach generated distribution estimated and employed a new quan-tile regression forest partitioning rule with a cost-sensitive decision-making structure, achieving superior prediction perfor-mance compared to traditional commitment times. [13] proposed the Graph2Route model, a dynamic spatial-temporal graph-based model leveraging underlying graph structure and features for encoding and decoding. Demonstrating superiority over existing models, Graph2Route captured evolving relationships between different problem instances, offering promising prospects for route optimization.

3. Methodology

3.1. Support Vector Machines

SVM is a supervised learning technique utilized in high-dimensional space to discern a hyperplane effectively segregating data points, enabling their analysis for both regression and classification purposes. In the pursuit of segregating distinct catego-ries of data points, SVM may utilize various hyperplanes. The principal objective of the algorithm is to ascertain the hyper-plane maximizing the margin, defined as the largest separation distance between data points belonging to different classes [14].

3.2. Light Gradient Boosting Machine

The LightGBM, a gradient-boosting framework, leverages tree-based learning methods. Distinguished from its predecessors, it offers several advantages, including accelerated processing, minimal RAM usage, support for parallel GPU learning, and heightened computational velocity. Employing a histogram-based approach, LightGBM efficiently segregates discrete-value continuous variables to mitigate processing costs. The granularity of divisions required for computation significantly impacts the training duration of decision trees. LightGBM optimizes resource consumption and expedites training by iteratively partitioning the tree per leaf and selecting the leaf with the maximal reduction in loss, thereby averting overfitting despite potential complexities inherent in smaller datasets [15].

3.3. Categorical Boosting

CatBoost, an open-source machine learning methodology rooted in GB, stands out within the field. Its notable attributes include rapid learning convergence, adept handling of diverse data types such as text, categorical, and numeric variables, compatibility with GPU acceleration, and comprehensive visualization capabilities, distinguishing it from conventional methods. Furthermore, CatBoost excels in the classification of categorical data and adeptly manages missing values without necessitating supplementary coding interventions during the data preprocessing phase [16].

3.4. Extreme Learning Machine

ELM stands as a training algorithm exhibiting promising performance particularly within the realm of single-hidden-layer Feed Forward Neural Networks (FFNN). It manifests notably expedited convergence in contrast to traditional methodolo-gies [17]. Diverging from conventional FFNN learning paradigms, such as the Back Propagation Algorithm (BPA), ELM eschews reliance on gradient-based techniques. Notably, it obviates the need for iterative training, as all model parameters are deterministically established in a single pass during the learning process.

3.5. Decision Tree

DT approach represents a supervised machine learning technique applicable to problems encompassing both regression (for continuous output values) and classification (for discrete output values). Its nomenclature derives from the tree-like structure, wherein features (or conditions) serve as branches, while class labels constitute the terminal nodes or leaves. The principal strength of DT lies in its inherent simplicity, interpretability, and visualizability. Moreover, it accommodates the integration of decision-making processes within the tree framework. Notably, this approach is adept at modeling datasets characterized by intricate nonlinear relationships between input and output variables. However, it is pertinent to acknowledge its suscepti-bility to overfitting and its limited efficacy in handling classification tasks involving multiple output classes [18].

4. Dataset Overview

The dataset obtained from Kaggle [19] consists of 5113 rows, containing historical delivery data for the 16-month period between February 14, 2019, and June 13, 2020. Categorical variables in the dataset have been converted to numerical values using One-Hot Coding. The features and their descriptions are presented in Table 1.

Table 1. Features in the Dataset

Feature Name	Definition
Year	Year
Month	Month of the year
Day	Day of the month
Hour	Hour of the day
Minute	Minute of the hour
Second	Second of the minute
PuP	Pick up point
DoP	Drop off point
Source_country	Country from where the product needs to be delivered
Destination_country	Country to where the product needs to be delivered
Freight_cost	Cost of transportation / kg
Gross_weight	Gross weight in kg which needs to be delivered
Delivery_charges	Fixed cost per delivery
Delivery_mode	Method of delivery
Delivering_company	Candidate delivering company
Shipping_time	The time that it takes for a product to reach their destination

5. Delivery Time Prediction Models

Models have been developed using CatBoost, DT, ELM, LightGBM and SVM to predict delivery times. 5-fold cross validation has been applied for each method. To increase the model's success, the optimal values of the specified hyperparameters have been found using grid search. The developed models have been evaluated using the MAPE metric since delivery time prediction is a regression problem. The hyperparameter ranges used as a basis for developing prediction models are given in Table 2.

Table 2. Hyperparameter Ranges

Methods	Hyperparameter Range
CatBoost	"Max_Depth": [5, 16] "Iterations": [3, 4] "Learning_Rate": [0.6, 1.0]
DT	"Max_Depth": [5, 12] "Min_Samples_Split": [2, 4] "Min_Samples_Leaf": [1, 4]
ELM	"Alpha": [0.1, 0.4] "Neuron_Size": [25, 75]
LightGBM	"N_Estimators": [75, 130] "Max_Depth": [5, 10] "Learning_Rate": [0.1, 0.2]
SVM	"Nu": [0.5, 0.9] "C": [1, 7] "Degree": [3]

6. Results and Discussion

The MAPE's obtained with the developed prediction models are given in Table 3.

Table 3. MAPE's of Delivery Time Prediction Models

	CatBoost	DT	ELM	LightGBM	SVM
1. Fold	21.23%	19.55%	21.94%	23.21%	19.61%
2. Fold	21.18%	19.29%	23.23%	23.95%	19.02%
3. Fold	21.57%	18.43%	22.74%	24.98%	18.04%
4. Fold	19.93%	19.36%	23.7%	19.5%	18.95%
5. Fold	18.98%	20.75%	20.78%	19.98%	18.06%
Average	20.58%	19.48%	22.48%	22.32%	18.74%

- The performance of SVM-based prediction model is 1.84% higher than that of CatBoost-based prediction model.
- SVM-based prediction model provided 3.74% lower MAPE than ELM-based prediction model.
- LightGBM-based prediction model has 3.58% higher MAPE than SVM-based prediction model.
- The DT-based prediction model shows a performance close to the SVM-based prediction model with a difference of 0.74%.
- The performance of DT-based prediction model is 1.1% higher than that of CatBoost-based prediction model.
- ELM and LightGBM-based prediction models have 3% and 2.84% higher MAPE, respectively, than DT-based prediction model.

Upon examination of the obtained results, it has been observed that, in general, the models developed using SVM exhibited the most successful prediction performance. ELM has been the model with the lowest performance and the highest MAPE among the developed forecasting models. As a result of the analysis, it has been observed that SVM and DT models provide satisfactory results in delivery time prediction.

7. Conclusion

Today, e-commerce has gained rapid momentum with large sales volumes. Consequently, the number of deliveries has also increased. To accurately plan the increasing number of delivery, the duration of these deliveries must be predicted. Logistics optimization can be achieved by planning the cargo delivery time, and customer satisfaction can be maximized by providing information about when the cargo will be delivered. In this study, the performance of different machine learning methods on cargo delivery time prediction have been compared. The prediction models have been evaluated with the MAPE metric. When the

results obtained from the developed prediction models have been examined, it has been found that SVM had superior performance in predicting delivery times.

References

[1] Nodirovna, M. S., & Sharif o'g'li, A. S. (2024). E-Commerce Trends: Shaping The Future of Retail. Open Herald: Periodical of Methodical Research, 2(3), 46-49.

[2] Muñoz-Villamizar, A., Velázquez-Martínez, J. C., Haro, P., Ferrer, A., & Mariño, R. (2021). The environmental impact of fast shipping ecommerce in inbound logistics operations: A case study in Mexico. Journal of Cleaner Production, 283, 125400.

[3] Cui, R., Lu, Z., Sun, T., & Golden, J. M. (2024). Sooner or later? Promising delivery speed in online retail. Manufacturing & Service Operations Management, 26(1), 233-251.

[4] Özdemir, R., Taşyürek, M., & Aslantaş, V. (2024). Improved Marine Predators Algorithm and Extreme Gradient Boosting (XGBoost) for shipment status time prediction. Knowledge-Based Systems, 111775.

[5] Zhang, L., Liu, Y., Zeng, Z., Cao, Y., Wu, X., Xu, Y., ... & Cui, L. (2024). Package Arrival Time Prediction via Knowledge Distillation Graph Neural Network. ACM Transactions on Knowledge Discovery from Data, 108: 1–19.

[6] Zhang, L., Wu, X., Liu, Y., Zhou, X., Cao, Y., Xu, Y., ... & Miao, C. (2024). Estimating package arrival time via heterogeneous hypergraph neural network. Expert Systems with Applications, 238, 121740.

[7] [Guo, B., Zuo, W., Wang, S., Zhou, X., & He, T. (2023). Attention Enhanced Package Pick-Up Time Prediction via Heterogeneous Behavior Modeling. In International Conference on Algorithms and Architectures for Parallel Pro-cessing Singapore: Springer Nature Singapore,189-208.

[8] Hamdan, I. K., Aziguli, W., Zhang, D., & Sumarliah, E. (2023). Machine learning in supply chain: prediction of real-time e-order arrivals using ANFIS. International Journal of System Assurance Engineering and Management, 14,Suppl 1, 549-568.

[9] Zhang, L., Zhou, X., Zeng, Z., Cao, Y., Xu, Y., Wang, M., ... & Shen, Z. (2023). Delivery time prediction using large-scale graph structure learning based on quantile regression. In 2023 IEEE 39th International Conference on Data Engineering, IEEE, 3403-3416.

[10] Zhou, X., Wang, J., Liu, Y., Wu, X., Shen, Z., & Leung, C. (2023). Inductive graph transformer for delivery time estimation. In Proceedings of the Sixteenth ACM International Conference on Web Search and Data Mining, 679-687.

[11] İnaç, H., Ayözen, Y. E., Atalan, A., & Dönmez, C. Ç. (2022). Estimation of postal service delivery time and energy cost with e-scooter by machine learning algorithms. Applied Sciences, 12(23), 12266.

[12] Salari, N., Liu, S., & Shen, Z. J. M. (2022). Real-time delivery time forecasting and promising in online retailing: When will your package arrive?. Manufacturing & Service Operations Management, 24(3), 1421-1436.

[13] Wen, H., Lin, Y., Mao, X., Wu, F., Zhao, Y., Wang, H., ... & Wan, H. (2022). Graph2route: A dynamic spatial-temporal graph neural network for pick-up and delivery route prediction. In Proceedings of the 28th ACM SIGKDD Conference On Knowledge Discovery and Data Mining, 4143-4152.

[14] Salcedo-Sanz, S., Rojo-Álvarez, J. L., Martínez-Ramón, M., & Camps-Valls, G. (2014). Support vector machines in engineering: an overview. Wiley Interdisciplinary Reviews: Data Mining and Knowledge Discovery, 4(3), 234-267.

[15] Barros, F. S., Cerqueira, V., & Soares, C. (2021). Empirical study on the impact of different sets of parameters of gradient boosting algorithms for time-series forecasting with LightGBM. In PRICAI 2021: Trends in Artificial Intelligence: 18th Pacific Rim International Conference on Artificial Intelligence, PRICAI 2021, Hanoi, Vietnam, November 8–12, 2021, Proceedings, Part I 18, Springer International Publishing, 454-465.

[16] Prokhorenkova, L., Gusev, G., Vorobev, A., Dorogush, A. V., & Gulin, A. (2018). CatBoost: unbiased boosting with categorical features. Advances in neural information processing systems, 31.

[17] Wang J., Lu S., Wang S. H., Zhang Y. D. (2022), A review on extreme learning machine, Multimedia Tools and Applications, 81(29), 41611-41660.

[18] Dabiri, H., Farhangi, V., Moradi, M. J., Zadehmohamad, M., & Karakouzian, M. (2022). Applications of decision tree and random forest as tree-based machine learning techniques for analyzing the ultimate strain of spliced and non-spliced reinforcement bars. Applied Sciences, 12(10), 4851.

[19] URL https://www.kaggle.com/datasets/salil007/1-shipping-optimization-challenge?select=train_2_pr.csv